

Chapter 2

Analysis of oscillation data

Observation of a variable star results in a determination of the variation of the properties of the star, such as the luminosity or the radial velocity, with time. To interpret the data, we need to isolate the properties of the underlying oscillations. When only a single mode is present, its period can normally be determined simply, and often very accurately. The analysis is much more complicated in the case of several modes, particularly when their amplitudes are small or their frequencies closely spaced. Here one has to use some form of Fourier analysis in time to isolate the frequencies that are present in the data.

For lack of better information, it was often assumed in the past that stellar oscillations have the simplest possible geometry, namely radial symmetry. This assumption is successful in many cases; however, radial oscillations are only a few among the many possible oscillations of a star, and the possible presence of nonradial modes must be kept in mind in analyses of oscillation observations (evidence for such modes in stars other than the Sun was summarized by Unno *et al.* 1989). A nonradial mode is characterized by three wavenumbers: the degree l and azimuthal order m which determine the behaviour of the mode over the surface of the star (see below) and the radial order n which reflects the properties in the radial direction (see Section 5.3). In general the frequencies ω_{nlm} of stellar oscillations depend on all three wave numbers. It is convenient, however, to separate the frequency into the *multiplet* frequency ω_{nl} , obtained as a suitable average over azimuthal order m and corresponding to the spherically symmetric structure of the star, and the *frequency splitting* $\delta\omega_{nlm} = \omega_{nlm} - \omega_{nl}$.

Analyses of oscillation data must attempt to separate these different frequency components. In the case of the Sun the oscillations can be observed directly as functions of position on the solar disk as well as time. Thus here it is possible to analyze their spatial properties. This is done by means of a generalized 2-dimensional Fourier transform in position on the solar surface, to isolate particular values of l and m . This is followed by a Fourier transform in time which isolates the frequencies of the modes of that type. In fact, the average over the stellar surface implicit in observations of stellar oscillations can be thought of as one example of such a spatial Fourier transform.

In this chapter I give a brief description of how the observable properties of the oscillations may be analyzed. The problems discussed here were treated in considerable detail by Christensen-Dalsgaard & Gough (1982). There are several books specifically on time-series analysis (*e.g.* Blackman & Tukey 1959; Bracewell 1978); an essentially “nuts-and-bolts”

description, with computer algorithms and examples, was given by Press *et al.* (1986). In addition, I summarize some observations of solar and stellar oscillations.

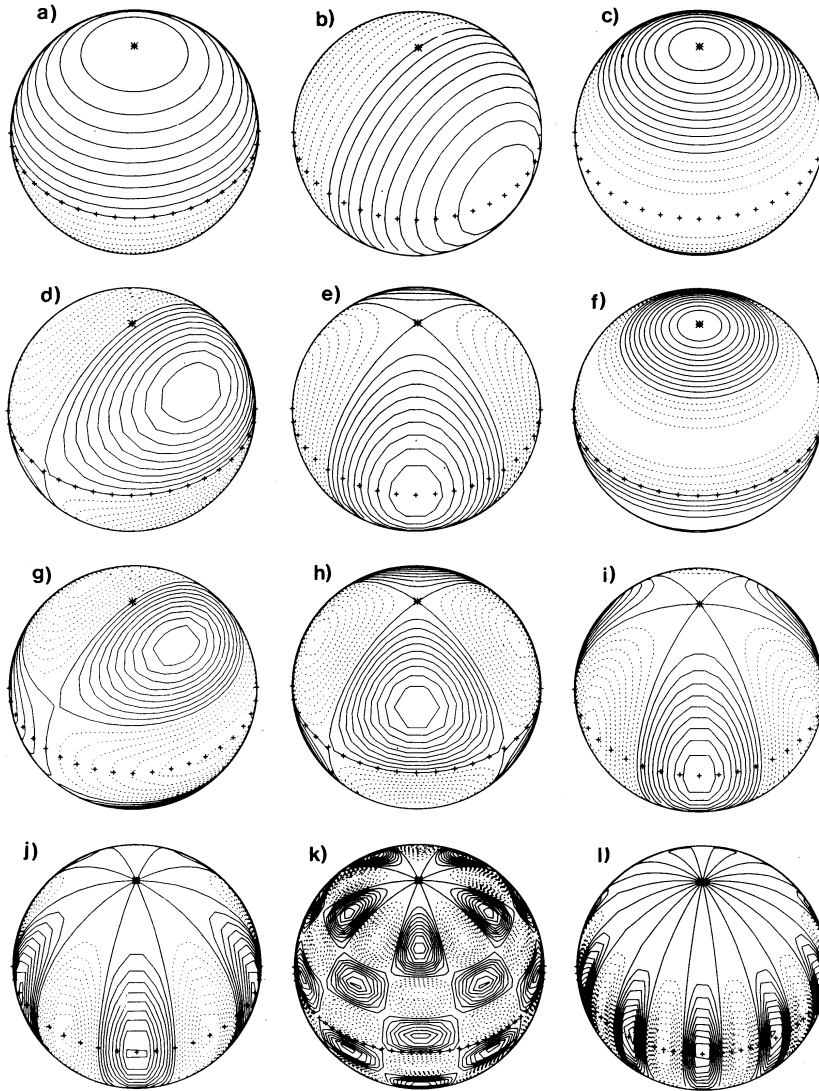


Figure 2.1: Contour plots of the real part of spherical harmonics Y_l^m [*cf.* equation (2.1); for simplicity the phase factor $(-1)^m$ has been suppressed]. Positive contours are indicated by continuous lines and negative contours by dashed lines. The $\theta = 0$ axis has been inclined by 45° towards the viewer, and is indicated by the star. The equator is shown by “++++”. The following cases are illustrated: a) $l = 1, m = 0$; b) $l = 1, m = 1$; c) $l = 2, m = 0$; d) $l = 2, m = 1$; e) $l = 2, m = 2$; f) $l = 3, m = 0$; g) $l = 3, m = 1$; h) $l = 3, m = 2$; i) $l = 3, m = 3$; j) $l = 5, m = 5$; k) $l = 10, m = 5$; l) $l = 10, m = 10$.

2.1 Spatial filtering

As shown in Chapter 4, small-amplitude oscillations of a spherical object like a star can be described in terms of spherical harmonics $Y_l^m(\theta, \phi)$ of co-latitude θ (*i.e.*, angular distance from the polar axis) and longitude ϕ . Here

$$Y_l^m(\theta, \phi) = (-1)^m c_{lm} P_l^m(\cos \theta) \exp(i m \phi), \quad (2.1)$$

where P_l^m is a Legendre function, and the normalization constant c_{lm} is determined by

$$c_{lm}^2 = \frac{(2l+1)(l-m)!}{4\pi(l+m)!}, \quad (2.2)$$

such that the integral of $|Y_l^m|^2$ over the unit sphere is 1. The degree l measures the total horizontal wave number k_h on the surface by

$$k_h = \frac{L}{R}, \quad (2.3)$$

where $L = \sqrt{l(l+1)}$, and R is the radius of the Sun. Equivalently the wavelength is

$$\lambda = \frac{2\pi}{k_h} = \frac{2\pi R}{L}. \quad (2.4)$$

Thus L is, roughly speaking, the number of wavelengths along the solar circumference. The azimuthal order m measures the number of nodes (*i.e.*, zeros) along the equator. The appearance of a few spherical harmonics is illustrated in Figure 2.1. Explicit expressions for selected Legendre functions, and a large number of useful results on their general properties, are given in Abramowitz & Stegun (1964). A summary is provided in Appendix A.

In writing down the spherical harmonics, I have left open the choice of polar axis. In fact, it is intuitively obvious that for a spherically symmetric star the choice of orientation of the coordinate system is irrelevant. If, on the other hand, the star is not spherically symmetric but possesses an axis of symmetry, this should be chosen as polar axis. The most important example of this is rotation, which is discussed in Chapter 8. In the present section I neglect departures from symmetry, and hence I am free to choose any direction of the polar axis.

Observations show that the solar oscillations consist of a superposition of a large number of modes, with degrees ranging from 0 to more than 1500. Thus here the observations and the data analysis must be organized so as to be sensitive to only a few degrees, to get time strings with contributions from sufficiently few individual oscillations that their frequencies can subsequently be resolved by Fourier analysis in time. The simplest form of mode isolation is obtained in whole-disk (or integrated-light) observations, where the intensity variations or velocity in light from the entire solar disk are observed. This corresponds to observing the Sun as a star, and, roughly speaking, averages out modes of high degree, where regions of positive and negative fluctuations approximately cancel.

To get a quantitative measure of the sensitivity of such observations to various modes, we consider first observations of intensity oscillations. The analysis in Chapter 4 shows that the oscillation in any scalar quantity, in particular the intensity, may be written on the form

$$\begin{aligned} I(\theta, \phi; t) &= \sqrt{4\pi} \Re \{ I_0 Y_l^m(\theta, \phi) \exp[-i(\omega_0 t - \delta_0)] \} \\ &= I_0 \sqrt{4\pi} (-1)^m c_{lm} P_l^m(\cos \theta) \cos(m\phi - \omega_0 t + \delta_0), \end{aligned} \quad (2.5)$$

where $\Re(z)$ is the real part of a complex quantity z . With the normalization chosen for the spherical harmonic, the *rms* of the intensity perturbation over the solar surface and time is $I_0/\sqrt{2}$. The response in whole-disk observations is obtained as the average over the disk of the Sun. Neglecting limb darkening, the result is

$$I(t) = \frac{1}{A} \int_A I(\theta, \phi; t) dA, \quad (2.6)$$

where A is area on the disk. To evaluate the integral, a definite choice of coordinate system is needed. As mentioned above, we are free to choose the computationally most convenient orientation, which is to have the polar axis point towards the observer. Then the integral is zero unless $m = 0$, and for $m = 0$

$$I(t) = S_l^{(I)} I_0 \cos(\omega_0 t - \delta_0), \quad (2.7)$$

where the spatial response function $S_l^{(I)}$ is

$$\begin{aligned} S_l^{(I)} &= \frac{1}{\pi} \int_0^{2\pi} d\phi \int_0^{\pi/2} \sqrt{2l+1} P_l(\cos \theta) \cos \theta \sin \theta d\theta \\ &= 2\sqrt{2l+1} \int_0^{\pi/2} P_l(\cos \theta) \cos \theta \sin \theta d\theta. \end{aligned} \quad (2.8)$$

This may be calculated directly for low l , or by recursion. Some results are shown in Figure 2.2.

Observations of the velocity oscillations are carried out by measuring the Doppler shift of spectral lines; hence such observations are only sensitive to the line-of-sight component of velocity. For low-degree modes with periods shorter than about an hour, the velocity field is predominantly in the radial direction [*cf.* equation (4.67)], and may be written as

$$V(\theta, \phi; t) = \sqrt{4\pi} \Re \{ V_0 Y_l^m(\theta, \phi) \exp[-i(\omega_0 t - \delta_0)] \mathbf{a}_r \}, \quad (2.9)$$

where \mathbf{a}_r is the unit vector in the radial direction. Here the *rms* over the solar surface and time of the radial component of velocity is $V_0/\sqrt{2}$. The result of whole-disk Doppler velocity observations may consequently be written, choosing again the polar axis to point towards the observer, as

$$v(t) = S_l^{(V)} V_0 \cos(\omega_0 t - \delta_0), \quad (2.10)$$

where

$$S_l^{(V)} = 2\sqrt{2l+1} \int_0^{\pi/2} P_l(\cos \theta) \cos^2 \theta \sin \theta d\theta \quad (2.11)$$

is the velocity response function. This differs from $S_l^{(I)}$ only by the factor $\cos \theta$ in the integrand, which is due to the projection of the velocity onto the line of sight. As a result the response is slightly larger at $l = 3$ than for intensity observations (see Figure 2.2).

The response corresponding to a different choice of polar axis can be obtained by direct integration of the spherical harmonics, with a different orientation, over the stellar disk. A simpler approach, however, is to note that there are transformation formulae connecting spherical harmonics corresponding to different orientations of the coordinate system (Edmonds 1960). An important special case is when the polar axis is in the plane of the

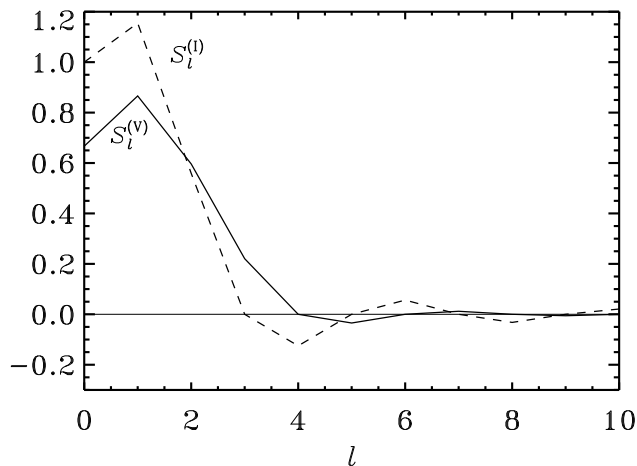


Figure 2.2: Spatial response functions $S_l^{(I)}$ and $S_l^{(V)}$ for observations of intensity and line-of-sight velocity, respectively, in light integrated over a stellar disk.

sky; this is approximately satisfied for the Sun, where the inclination of the rotation axis, relative to the sky, is at most about 7° . One then obtains the response as

$$S'_{lm} = \Gamma_{lm} S_l, \quad (2.12)$$

where S_l is the response as determined in equation (2.8) or (2.11), and the coefficients Γ_{lm} can be evaluated as described by Christensen-Dalsgaard & Gough (1982). In particular it is easy to see that Γ_{lm} is zero when $l - m$ is odd, for in this case the Legendre function $P_l^m(\cos \theta)$ is antisymmetric around the equator. Also $\Gamma_{l-m} = \Gamma_{lm}$. The non-trivial values of Γ_{lm} for the lowest degrees are:

$$\begin{aligned} \Gamma_{00} &= 1 \\ \Gamma_{11} &= \frac{1}{\sqrt{2}} \\ \Gamma_{20} &= \frac{1}{2} & \Gamma_{22} &= \frac{\sqrt{6}}{4} \\ \Gamma_{31} &= \frac{\sqrt{3}}{4} & \Gamma_{33} &= \frac{\sqrt{5}}{4} \end{aligned} \quad (2.13)$$

To isolate modes of higher degrees, one must analyse observations made as functions of θ and ϕ . Had data been available that covered the entire Sun, modes corresponding to a single pair (l_0, m_0) could in principle have been isolated by multiplying the data, after suitable scaling, with a spherical harmonic $Y_{l_0}^{m_0}(\theta, \phi)$ and integrating over the solar surface; it follows from the orthogonality of the spherical harmonics that the result would contain only oscillations corresponding to the degree and azimuthal order selected. In practice the observations are restricted to the visible disk of the Sun, and the sensitivity to velocity oscillations is further limited close to the limb due to the projection onto the line of sight.

To illustrate the principles in the mode separation in a little more detail, I note that, according to equations (2.1) and (2.9), the combined observed Doppler velocity on the solar surface is of the form

$$V_D(\theta, \phi, t) = \sin \theta \cos \phi \sum_{n,l,m} A_{nlm}(t) c_{lm} P_l^m(\cos \theta) \cos[m\phi - \omega_{nlm}t - \delta_{nlm}(t)]. \quad (2.14)$$

Now the axis of the coordinate system has been taken to be in the plane of the sky; longitude ϕ is measured from the central meridian. [Also, to simplify the notation the factor $(-1)^m \sqrt{4\pi}$ has been included in A_{nlm} .] For simplicity, I still assume that the velocity is predominantly in the radial direction, as is the case for five-minute oscillations of low or moderate degree; the factor $\sin \theta \cos \phi$ results from the projection of the velocity vector onto the line of sight. The amplitudes A_{nlm} and phases δ_{nlm} may vary with time, as a result of the excitation and damping of the modes.

As discussed above, it may be assumed that V_D has been observed as a function of position (θ, ϕ) on the solar surface. The spatial transform may be thought of as an integration of the observations multiplied by a weight function $W_{l_0 m_0}(\theta, \phi)$ designed to give greatest response to modes in the vicinity of $l = l_0, m = m_0$. The result is the filtered time string

$$\begin{aligned} V_{l_0 m_0}(t) &= \int_A V_D(\theta, \phi, t) W_{l_0 m_0}(\theta, \phi) dA \\ &= \sum_{n,l,m} S_{l_0 m_0 l m} A_{nlm} \cos[\omega_{nlm}t + \hat{\delta}_{nlm, l_0 m_0}]. \end{aligned} \quad (2.15)$$

Here, the integral is over area on the solar disk, and $dA = \sin^2 \theta \cos \phi d\theta d\phi$; also, I introduced the *spatial response function* $S_{l_0 m_0 l m}$, defined by

$$(S_{l_0 m_0 l m})^2 = \left(S_{l_0 m_0 l m}^{(+)} \right)^2 + \left(S_{l_0 m_0 l m}^{(-)} \right)^2, \quad (2.16)$$

where

$$S_{l_0 m_0 l m}^{(+)} = c_{lm} \int_A W_{l_0 m_0}(\theta, \phi) P_l^m(\cos \theta) \cos(m\phi) \sin \theta \cos \phi dA, \quad (2.17)$$

and

$$S_{l_0 m_0 l m}^{(-)} = c_{lm} \int_A W_{l_0 m_0}(\theta, \phi) P_l^m(\cos \theta) \sin(m\phi) \sin \theta \cos \phi dA. \quad (2.18)$$

The new phases $\hat{\delta}_{nlm, l_0 m_0}$ in equation (2.15) depend on the original phases δ_{nlm} and on $S_{l_0 m_0 l m}^{(+)}$ and $S_{l_0 m_0 l m}^{(-)}$.

It is evident that to simplify the subsequent analysis of the time string $V_{l_0 m_0}(t)$, it is desirable that it contain contributions from a limited number of spherical harmonics (l, m) . This is to be accomplished through a suitable choice of the weight function $W_{l_0 m_0}(\theta, \phi)$ such that $S_{l_0 m_0 l m}$ is large for $l = l_0, m = m_0$ and “small” otherwise. Indeed, it follows from the orthogonality of the spherical harmonics that, if $W_{l_0 m_0}$ is taken to be the spherical harmonic $Y_{l_0}^{m_0}$, if the integrals in equations (2.17) and (2.18) are extended to the full sphere, and if, in the integrals, $\sin \theta \cos \phi dA$ is replaced by $\sin \theta d\theta d\phi$, then essentially $S_{l_0 m_0 l m} \propto \delta_{l_0 l} \delta_{m_0 m}$. It is obvious that, with realistic observations restricted to one hemisphere of the Sun, this optimal level of concentration cannot be achieved. However, the result suggests that suitable weights can be obtained from spherical harmonics. Weights of this nature are almost always used in the analysis. The resulting response functions are typically of order

unity for $|l-l_0| \lesssim 2$, $|m-m_0| \lesssim 2$ and relatively small elsewhere (*e.g.* Duvall & Harvey 1983; Christensen-Dalsgaard 1984a); this is roughly comparable to the mode isolation achieved in whole disk observations. That the response extends over a range in l and m is analogous to the quantum-mechanical uncertainty principle between localization in space and momentum (here represented by wavenumber). If the area being analyzed is reduced, the spread in l and m is increased; conversely, intensity observations, which do not include the projection factor $\sin \theta \cos \phi$, effectively sample a larger area of the Sun and therefore, in general, lead to somewhat greater concentration in l and m (see also Fig. 2.2).

2.2 Fourier analysis of time strings

The preceding section considered the spatial analysis of oscillation observations, either implicitly through observation in integrated light or explicitly through a spatial transform. Following this analysis we are left with timestrings containing a relatively limited number of modes. These modes may then be separated through Fourier analysis in time. Here I mainly consider simple harmonic oscillations. These are typical of small-amplitude pulsating stars, such as the Sun. Some remarks on periodic oscillations with more complex behaviour are given in Section 2.2.5.

A simple harmonic oscillating signal can be written as

$$v(t) = a_0 \cos(\omega_0 t - \delta_0) . \quad (2.19)$$

Here ω_0 is the angular frequency, and the period of oscillation is $\Pi = 2\pi/\omega_0$. Oscillations are often also discussed in terms of their cyclic frequency $\nu = 1/\Pi = \omega/2\pi$, measured in mHz or μHz . A period of 5 minutes (typical of the most important class of solar oscillations) corresponds to $\nu = 3.3 \text{ mHz} = 3300 \mu\text{Hz}$, and $\omega = 0.021 \text{ s}^{-1}$. In studies of classical pulsating stars it is common to measure the period in units of the dynamical time scale t_{dyn} [*cf.* equation (1.1)] by representing it in terms of the *pulsation constant*

$$Q = \Pi \left(\frac{M}{M_\odot} \right)^{1/2} \left(\frac{R}{R_\odot} \right)^{-3/2} , \quad (2.20)$$

where M_\odot and R_\odot are the solar mass and radius. Thus Q provides information about the more intricate properties of stellar interior structure, beyond the simple scaling of the period with the dynamical time scale.

2.2.1 Analysis of a single oscillation

The signal in equation (2.19) is assumed to be observed from $t = 0$ to $t = T$. Then the Fourier transform is

$$\begin{aligned} \tilde{v}(\omega) &= \int_0^T v(t) e^{i\omega t} dt = \frac{1}{2} a_0 \int_0^T \left[e^{i(\omega_0 t - \delta_0)} + e^{-i(\omega_0 t - \delta_0)} \right] e^{i\omega t} dt \\ &= \frac{1}{2} a_0 \left\{ \frac{e^{-i\delta_0}}{i(\omega + \omega_0)} [e^{i(\omega + \omega_0)T} - 1] + \frac{e^{i\delta_0}}{i(\omega - \omega_0)} [e^{i(\omega - \omega_0)T} - 1] \right\} \\ &= a_0 \left\{ e^{i[T/2(\omega + \omega_0) - \delta_0]} \frac{\sin[T/2(\omega + \omega_0)]}{\omega + \omega_0} + e^{i[T/2(\omega - \omega_0) + \delta_0]} \frac{\sin[T/2(\omega - \omega_0)]}{\omega - \omega_0} \right\} \\ &= \frac{T}{2} a_0 \left\{ e^{i[T/2(\omega + \omega_0) - \delta_0]} \text{sinc} \left[\frac{T}{2} (\omega + \omega_0) \right] + e^{i[T/2(\omega - \omega_0) + \delta_0]} \text{sinc} \left[\frac{T}{2} (\omega - \omega_0) \right] \right\} , \end{aligned} \quad (2.21)$$

where

$$\text{sinc}(x) = \frac{\sin x}{x}. \quad (2.22)$$

Plots of $\text{sinc}(x)$ and $\text{sinc}^2(x)$ are shown in Figure 2.3. The power spectrum is

$$P(\omega) = |\tilde{v}(\omega)|^2 \quad (2.23)$$

and has the appearance shown schematically in Figure 2.4.

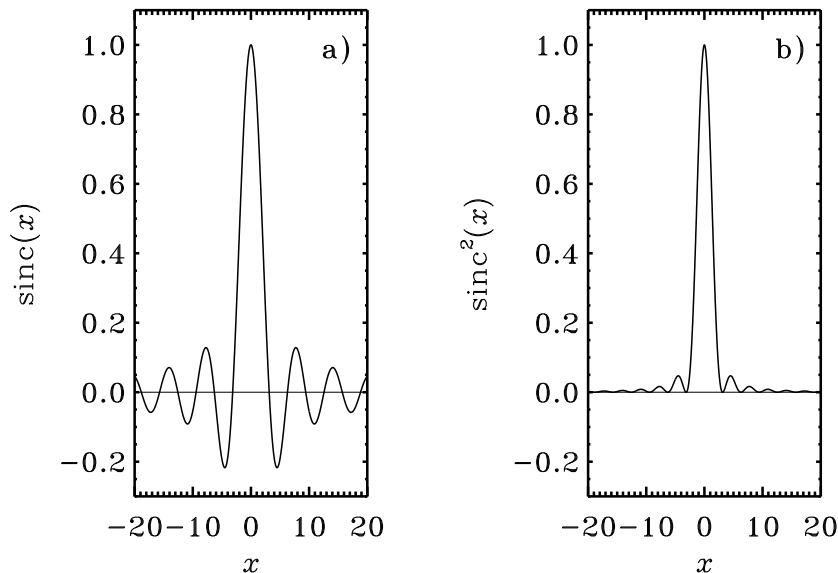


Figure 2.3: The sinc function (a) and sinc^2 function (b) [*cf.* equation (2.22)].

If $T\omega_0 \gg 1$ the two components of the spectrum at $\omega = -\omega_0$ and $\omega = \omega_0$ are well separated, and we need only consider, say, the positive ω -axis; then, approximately

$$P(\omega) \simeq \frac{1}{4} T^2 a_0^2 \text{sinc}^2 \left[\frac{T}{2} (\omega - \omega_0) \right]. \quad (2.24)$$

I use this approximation in the following. Then both the maximum and the centre of gravity of P is at $\omega = \omega_0$. Thus in principle both quantities can be used to determine the frequencies from observations of oscillation. In practice the observed peak often has a more complex structure, due to observational noise and fluctuations in the oscillation amplitude. In such cases the centre of gravity is often better defined than the location of the maximum of the peak. As a measure of the accuracy of the frequency determination, and of the ability to separate closely spaced peaks, we may use the width $\delta\omega$ of the peak, which may be estimated by, say

$$\frac{T}{2} \frac{\delta\omega}{2} \simeq \frac{\pi}{2}, \quad \delta\omega \simeq \frac{2\pi}{T}, \quad \delta\nu \simeq \frac{1}{T}. \quad (2.25)$$

(More precisely, the half width at half maximum of $\text{sinc}^2(x)$ is 0.443π .) Hence to determine the frequency accurately, we need extended observations (T must be large.) In fact, the relative resolution

$$\frac{\delta\omega}{\omega_0} \simeq \frac{2\pi}{\omega_0 T} = \frac{\Pi}{T} \quad (2.26)$$

is 1 divided by the number of oscillation periods during the observing time T . Note also that for 8 hours of observations (a typical value for observations from a single site) the width in cyclic frequency is $\delta\nu = 34 \mu\text{Hz}$.

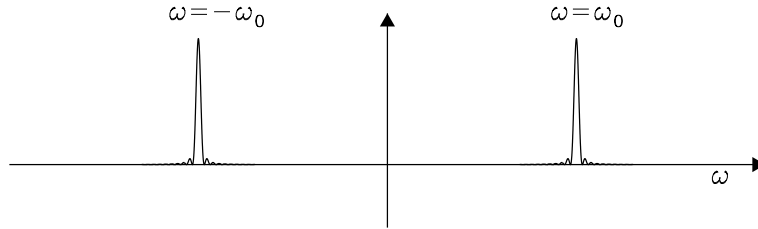


Figure 2.4: Schematic appearance of the power spectrum of a single harmonic oscillation. Note that the oscillation gives rise to a peak on both the positive and the negative ω -axis.

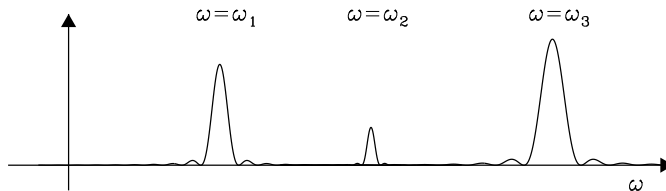


Figure 2.5: Schematic representation of spectrum containing 3 well-separated modes.

2.2.2 Several simultaneous oscillations

Here the time string is

$$v(t) = a_1 \cos(\omega_1 t - \delta_1) + a_2 \cos(\omega_2 t - \delta_2) + a_3 \cos(\omega_3 t - \delta_3) + \dots \quad (2.27)$$

The spectrum might be expected to be, roughly, the sum of the spectra of the individual oscillations, as shown schematically in Figure 2.5. This would allow the individual frequencies to be determined. This is the case if the modes are well separated, with $|\omega_i - \omega_j|T \gg 1$ for all pairs $i \neq j$. However, in the Sun and other types of pulsating stars the oscillation

frequencies are densely packed, and the situation may be a great deal more complicated. I consider the case of just two oscillations in more detail:

$$v(t) = a_1 \cos(\omega_1 t - \delta_1) + a_2 \cos(\omega_2 t - \delta_2) . \quad (2.28)$$

Then on the positive ω -axis we get the Fourier transform

$$\begin{aligned} \tilde{v}(\omega) \simeq & \quad (2.29) \\ \frac{T}{2} \left\{ a_1 e^{i[T/2(\omega - \omega_1) + \delta_1]} \text{sinc} \left[\frac{T}{2}(\omega - \omega_1) \right] + a_2 e^{i[T/2(\omega - \omega_2) + \delta_2]} \text{sinc} \left[\frac{T}{2}(\omega - \omega_2) \right] \right\} , \end{aligned}$$

and the power

$$\begin{aligned} P(\omega) = & \quad (2.30) \\ \frac{T^2}{4} \left\{ a_1^2 \text{sinc}^2 \left[\frac{T}{2}(\omega - \omega_1) \right] + a_2^2 \text{sinc}^2 \left[\frac{T}{2}(\omega - \omega_2) \right] \right. \\ & \left. + 2a_1 a_2 \text{sinc} \left[\frac{T}{2}(\omega - \omega_1) \right] \text{sinc} \left[\frac{T}{2}(\omega - \omega_2) \right] \cos \left[\frac{T}{2}(\omega_2 - \omega_1) - (\delta_2 - \delta_1) \right] \right\} . \end{aligned}$$

Note that a naive summation of the two individual spectra would result in the first two terms; the last term is caused by *interference* between the modes, which is very important for closely spaced frequencies. The outcome depends critically on the relative phases, and to some extent the relative amplitudes, of the oscillations.

In Figure 2.6 are shown some examples of spectra containing two oscillations. Here, to limit the parameter space, $a_1 = a_2$. $\Delta\omega = \omega_2 - \omega_1$ is the frequency difference (which is non-negative in all cases), and $\Delta\delta = \delta_2 - \delta_1$ is the phase difference at $t = 0$. The vertical lines show the locations of the frequencies ω_1 and ω_2 . Note in particular that when $\Delta\delta = 3\pi/2$, the splitting is artificially exaggerated when $\Delta\omega$ is small; the peaks in power are shifted by considerable amounts relative to the actual frequencies. This might easily cause confusion in the interpretation of observed spectra. These effects were discussed by Loumos & Deeming (1978) and analyzed in more detail by Christensen-Dalsgaard & Gough (1982). From the results in Figure 2.6 we obtain the rough estimate of the frequency separation that can be resolved in observations of duration T regardless of the relative phase:

$$\delta\omega \simeq \frac{12}{T} . \quad (2.31)$$

Note that this is about twice as large as the width of the individual peaks estimated in equation (2.25).

To demonstrate in more detail the effect on the observed spectrum of the duration of the time series, I consider the analysis of an artificial data set with varying resolution, for the important case of low-degree, high-order p modes of a rotating star. I use a simplified approximation to the asymptotic theory presented in Chapter 7 [*cf.* equations (7.55) and (7.58)], and the discussion of the effects of rotation in Chapter 8 [*cf.* equation (8.45)], and hence approximate the frequencies of such modes as

$$\nu_{nlm} \simeq \Delta\nu_0 \left(n + \frac{l}{2} + \epsilon_0 \right) - l(l+1)D_0 + m\Delta\nu_{\text{rot}} , \quad (2.32)$$

where n is the radial order (*i.e.*, the number of nodes in the radial direction), and l and m were defined in Section 2.1. Here the last term is caused by rotation, with $\Delta\nu_{\text{rot}} = 1/\Pi_{\text{rot}}$, where Π_{rot} is an average over the star of the rotation period. The remaining

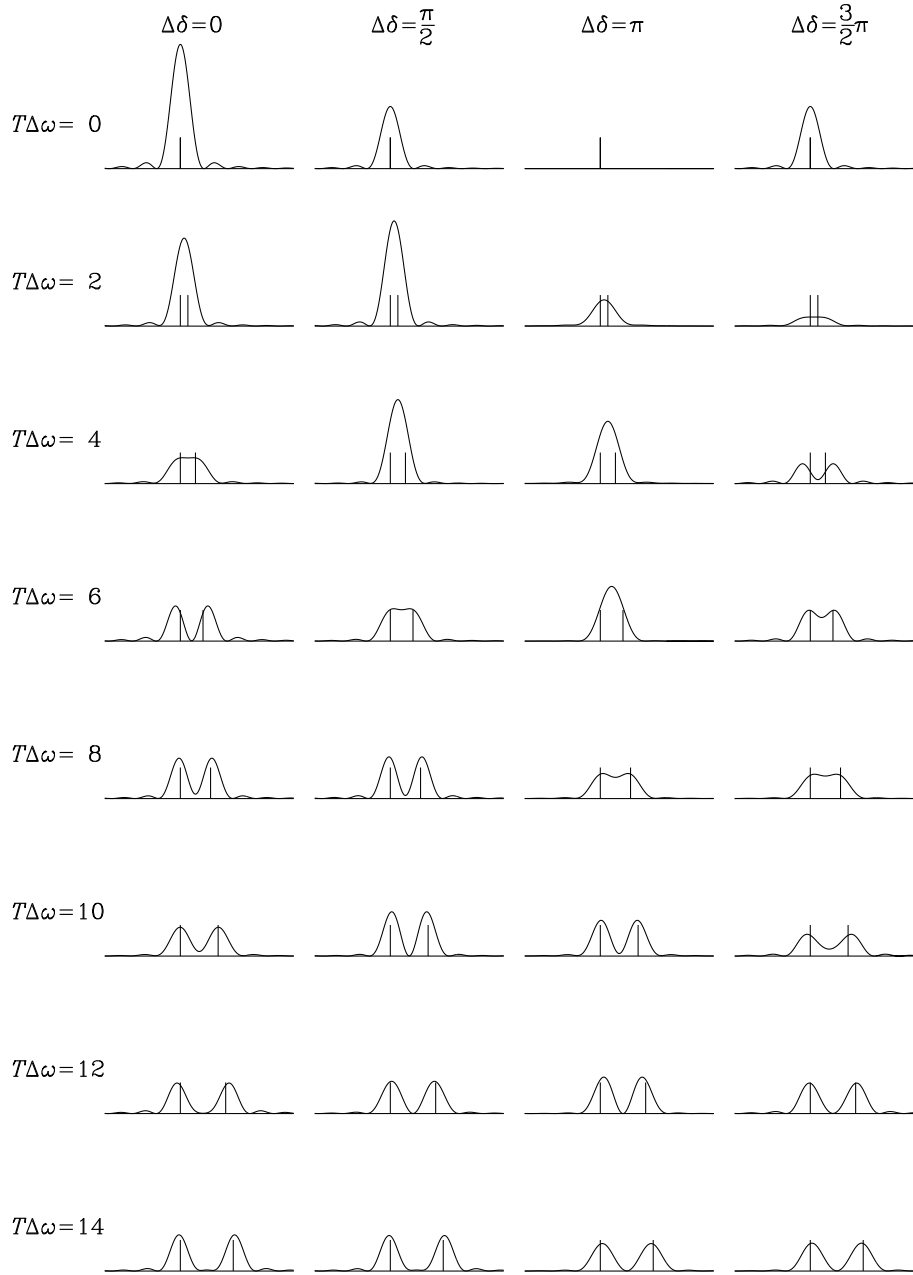


Figure 2.6: Spectra of two modes closely spaced in frequency, with the same amplitude [*cf.* equation (2.30)]. The vertical lines the frequency and amplitude of the two modes. $\Delta\omega = \omega_2 - \omega_1$ is the frequency difference between the modes, and $\Delta\delta = \delta_2 - \delta_1$ is the phase difference at $t = 0$.

terms approximate the frequencies of the nonrotating star. The dominant term is the first, according to which the frequencies depend predominantly on n and l in the combination $n + l/2$. Thus to this level of precision the modes are organized in groups according to the

parity of l . The term in $l(l+1)$ causes a separation of the frequencies according to l , and finally the last term causes a separation, which is normally considerably smaller, according to m . There is an evident interest in being able to resolve these frequency separations observationally.

The frequencies were calculated from equation (2.32), with $\Delta\nu_0 = 120 \mu\text{Hz}$, $\epsilon_0 = 1.2$, $D_0 = 1.5 \mu\text{Hz}$ and a rotational splitting $\Delta\nu_{\text{rot}} = 1 \mu\text{Hz}$ (corresponding to about twice the solar surface rotation rate). These values are fairly typical for solar-like stars. The response of the observations to the modes was calculated as described in Section 2.1; for simplicity the rotation axis was assumed to be in the plane of the sky, so that only modes with even $l-m$ can be observed. For clarity the responses for $l=3$ were increased by a factor 2.5. The amplitudes and phases of the modes were chosen randomly, but were the same for all time strings. The data were assumed to be noise-free.

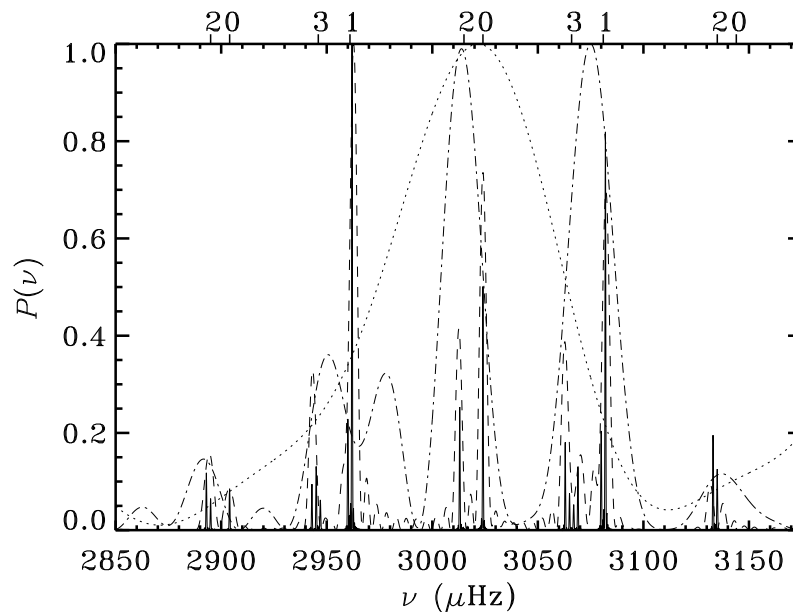


Figure 2.7: Power spectra of simulated time series of duration 600 h (—), 60 h (-----), 10 h (-·-·-·-·-) and 3 h (······). The power is on an arbitrary scale and has been normalized to a maximum value of 1. The location of the central frequency for each group of rotationally split modes, as well as the value of the degree, are indicated on the top of the diagram. (From Christensen-Dalsgaard 1984b.)

Short segments of the resulting power spectra, for $T = 3$ h, 10 h, 60 h and 600 h, are shown in Figure 2.7. The power is on an arbitrary scale, normalized so that the maximum is unity in each case. For $T = 600$ h the modes are completely resolved. At $T = 60$ h the rotational splitting is unresolved, but the modes at individual n and l can to a large extent be distinguished; however, a spurious peak appears next to the dominant peak with $l = 1$ at $2960 \mu\text{Hz}$. For $T = 10$ h modes having degrees of the same parity merge; here

the odd- l group at $\nu \simeq 2960 \mu\text{Hz}$ gives rise to two clearly resolved, but fictitious, peaks of which one is displaced by about $20 \mu\text{Hz}$ relative to the centre of the group. These effects are qualitatively similar to those seen in Figure 2.6. Finally, the spectrum for $T = 3 \text{ h}$ is dominated by interference and bears little immediate relation to the underlying frequencies.

The case shown in Figure 2.7 was chosen as typical among a fairly large sample with different random phases and amplitudes. The results clearly emphasize the care that is required when interpreting inadequately resolved data. Furthermore, in general all values of m are expected to be observed for stellar oscillations, adding to the complexity.

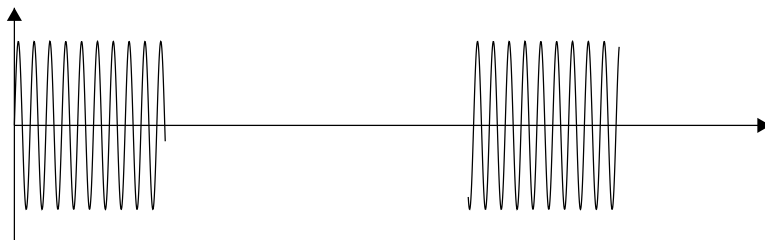


Figure 2.8: Sketch of interrupted time series. This corresponds to two 8 hour data segments, separated by a 16 hour gap.

2.2.3 Data with gaps

From a single site (except very near one of the poles) the Sun or a star can typically be observed for no more than 10–12 hours out of each 24 hours. As discussed in connection with Figure 2.7, this is far from enough to give the required frequency resolution. Thus one is faced with combining data from several days. This adds confusion to the spectra. I consider again the signal in equation (2.19), but now observe it for $t = 0$ to T and τ to $\tau + T$. The signal is unknown between T and τ , and it is common to set it to zero here, as sketched in Figure 2.8. Then the Fourier transform is, on the positive ω -axis,

$$\begin{aligned} \tilde{v}(\omega) &= \int_0^T v(t) e^{i\omega t} dt + \int_\tau^{\tau+T} v(t) e^{i\omega t} dt \\ &\simeq \frac{T}{2} a_0 \left\{ e^{i[\frac{T}{2}(\omega - \omega_0) + \delta_0]} + e^{i[(\tau + \frac{T}{2})(\omega - \omega_0) + \delta_0]} \right\} \text{sinc} \left[\frac{T}{2}(\omega - \omega_0) \right] \\ &= T a_0 e^{i[1/2(\tau + T)(\omega - \omega_0) + \delta_0]} \cos \left[\frac{T}{2}(\omega - \omega_0) \right] \text{sinc} \left[\frac{T}{2}(\omega - \omega_0) \right], \end{aligned} \quad (2.33)$$

and the power is

$$P(\omega) = T^2 a_0^2 \cos^2 \left[\frac{T}{2}(\omega - \omega_0) \right] \text{sinc}^2 \left[\frac{T}{2}(\omega - \omega_0) \right]. \quad (2.34)$$

Thus one gets the spectrum from the single-day case, modulated by the $\cos^2[\frac{1}{2}\tau(\omega - \omega_0)]$ factor. As $\tau > T$ this introduces apparent fine structure in the spectrum. An example with $\tau = 3T$ is shown in Figure 2.9.

When more days are combined this so-called side-band structure can be somewhat suppressed, but never entirely removed. In particular, there generally remain two additional

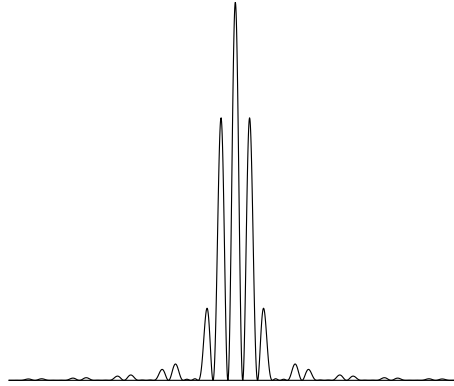


Figure 2.9: Power spectrum of the time series shown in Figure 2.8 [cf. equation (2.34)].

peaks separated from the main peak by $\delta\omega = 2\pi/\tau$ or $\delta\nu = 1/\tau$. For $\tau = 24$ hours, $\delta\nu = 11.57 \mu\text{Hz}$.

Exercise 2.1:

Evaluate the power spectrum for the signal in equation (2.19), observed between 0 and T , τ and $\tau + T$, ... $N\tau$, $N\tau + T$, and verify the statement made above.

If several closely spaced modes are present as well, the resulting interference may get quite complicated, and the interpretation correspondingly difficult. An example of this is shown in Figure 2.10, together with the corresponding spectrum resulting from a single day's observations.

The effects of gaps can conveniently be represented in terms of the so-called *window function* $w(t)$, defined such that $w(t) = 1$ during the periods with data and $w(t) = 0$ during the gaps. Thus the observed data can be written as

$$v(t) = w(t)v_0(t), \quad (2.35)$$

where $v_0(t)$ is the underlying signal (which, we assume, is there whether it is observed or not). It follows from the convolution theorem of Fourier analysis that the Fourier transform of $v(t)$ is the convolution of the transforms of $v_0(t)$ and $w(t)$:

$$\tilde{v}(\omega) = (\tilde{w} * \tilde{v}_0)(\omega) = \int \tilde{w}(\omega - \omega')\tilde{v}_0(\omega')d\omega'; \quad (2.36)$$

here '*' denotes convolution, and $\tilde{w}(\omega)$ is the transform of a timestring consisting of 0 and 1, which is centred at zero frequency. It follows from equation (2.36) that if the peaks in the original power spectrum $P_0(\omega) = |\tilde{v}_0(\omega)|^2$ are well separated compared with the spread

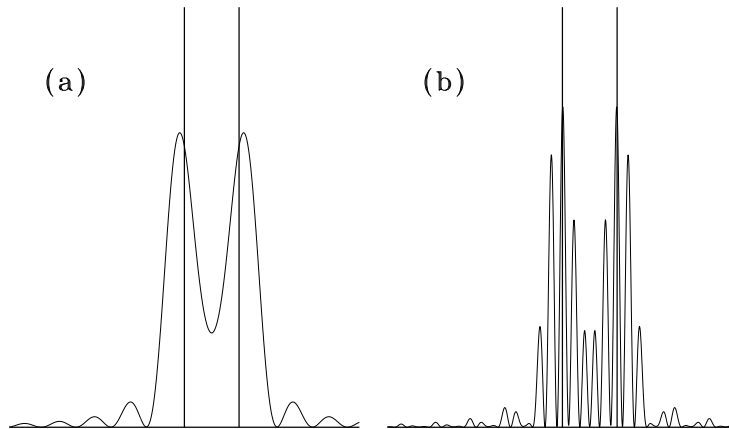


Figure 2.10: In (a) is shown the spectrum for two closely spaced modes with $T\Delta\omega = 10$, $\Delta\delta = 3\pi/2$, observed during a single day, from Figure 2.6. In (b) is shown the corresponding case, but observed for two 8 hour segments separated by 24 hours.

of the window function transform $P_w(\omega) = |\tilde{w}(\omega)|^2$, the observed spectrum $P(\omega) = |\tilde{v}(\omega)|^2$ consists of copies of $P_w(\omega)$, shifted to be centred on the ‘true’ frequencies. Needless to say, the situation becomes far more complex when the window function transforms overlap, resulting in interference.

There are techniques that to some extent may compensate for the effects of gaps in the data, even in the presence of noise (*e.g.* Brown & Christensen-Dalsgaard 1990). However, these are relatively inefficient when the data segments are shorter than the gaps. To overcome these problems, several independent projects are under way to construct networks of observatories with a suitable distribution of sites around the Earth, to study solar oscillations with minimal interruptions. Campaigns to coordinate observations of stellar oscillations from different observatories have also been organized. Furthermore, the SOHO spacecraft has carried helioseismic instruments to the L_1 point between the Earth and the Sun, where the observations can be carried out without interruptions. This has the added advantage of avoiding the effects of the Earth’s atmosphere.

2.2.4 Further complications

The analysis in the preceding sections is somewhat unrealistic, in that it is assumed that the oscillation amplitudes are strictly constant. If the oscillation is damped, one has, instead of equation (2.19)

$$v(t) = a_0 \cos(\omega_0 t - \delta_0) e^{-\eta t}, \quad (2.37)$$

where η is the *damping rate*. If this signal is observed for an infinitely long time, one obtains the power spectrum

$$P(\omega) = \frac{1}{4} \frac{a_0^2}{(\omega - \omega_0)^2 + \eta^2}. \quad (2.38)$$

A peak of this form is called a *Lorentzian profile*. It has a half width at half maximum of η .

Exercise 2.2:

Verify equation (2.38).

If the signal in equation (2.37) is observed for a finite time T , the resulting peak is intermediate between the sinc^2 function and the Lorentzian, tending to the former for $\eta T \ll 1$, and towards the latter for $\eta T \gg 1$. This transition is illustrated in Figure 2.11.

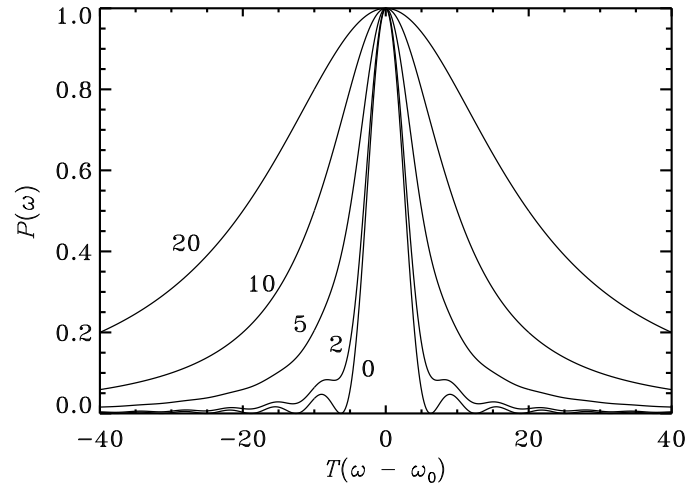


Figure 2.11: Power spectrum for the damped oscillator in equation (2.37), observed for a finite time T . The abscissa is frequency separation, in units of T^{-1} . The ordinate has been normalized to have maximum value 1. The curves are labelled by the value of ηT , where η is the damping rate.

Equation (2.37) is evidently also an idealization, in that it (implicitly) assumes a sudden excitation of the mode, followed by an exponential decay. In the Sun, at least, it appears that the oscillations are excited stochastically, by essentially random fluctuations due to the turbulent motion in the outer parts of the solar convection zone. It may be shown that this process, combined with exponential decay, gives rise to a spectrum that on average has a Lorentzian profile. The statistics of the determination of frequencies, amplitudes and line widths from such a spectrum was studied by Sørensen (1988), Kumar, Franklin & Goldreich (1988) and Schou (1993). These issues are discussed in more detail in Section 10.3. It should be noted (see also Figure 10.4) that the stochastic nature of the excitation gives rise to a number of sharp peaks, with a distribution around the the general Lorentzian envelope; thus, in particular, it cannot be assumed that the maximum power corresponds to the true frequency of the mode. Substantial care is therefore required in analyzing data of this nature.

So far I have considered only noise-free data. Actual observations of oscillations contain noise from the observing process, from the Earth's atmosphere and from the random velocity

(or intensity) fields in the solar or stellar atmosphere. At each frequency in the power spectrum the noise may be considered as an oscillation with a random amplitude and phase; this interferes with the actual, regular oscillations, and may suppress or artificially enhance some of the oscillations. However, because the noise is random, it may be shown to decrease in importance with increasingly long time series.

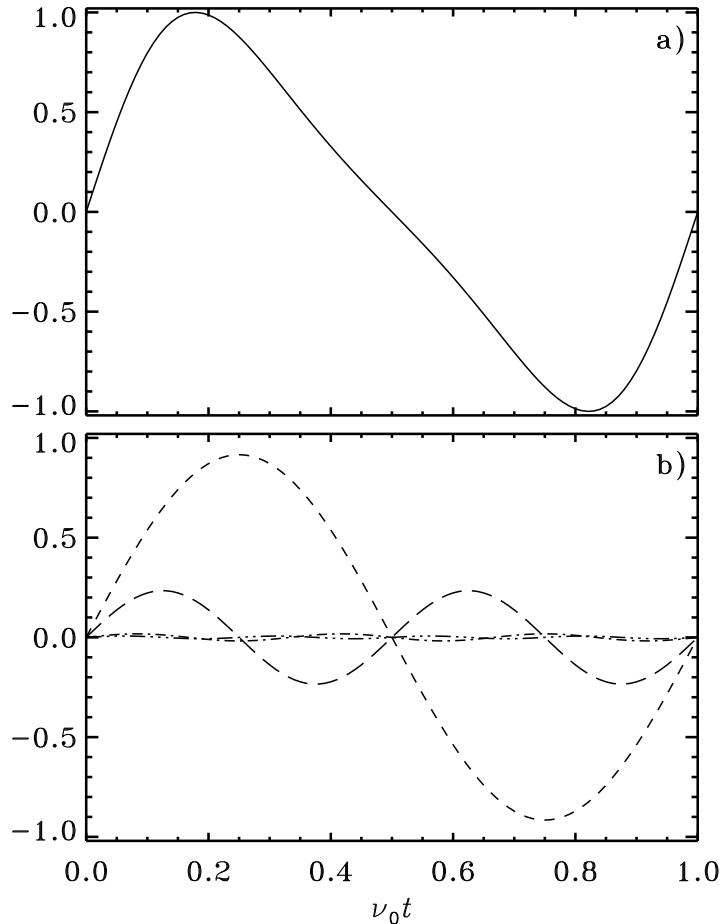


Figure 2.12: (a) Example of non-sinusoidal oscillation, plotted against relative phase $\nu_0 t = \omega_0 t / 2\pi$. This is roughly similar to observed light curves of large-amplitude Cepheids. (b) The first 3 Fourier components of the oscillation shown in panel (a). The remaining components have so small amplitudes that they do not contribute significantly to the total signal.

2.2.5 Large-amplitude oscillations

For large-amplitude pulsating stars, such as Cepheids, the oscillation typically no longer behaves like the simple sine function in equation (2.19). Very often the oscillation is still strictly periodic, however, with a well-defined frequency ω_0 . Also the light curve, for example, in many cases has a shape similar to the one shown in Figure 2.12, with a rapid rise

and a more gradual decrease.

It is still possible to carry out a Fourier analysis of the oscillation. Now, however, peaks appear at the harmonics $k\omega_0$ of the basic oscillation frequency, where $k = 1, 2, \dots$. This corresponds to representing the observed signal as a Fourier series

$$v(t) = \sum_k a_k \sin(k\omega_0 t - \phi_k). \quad (2.39)$$

Figure 2.12b shows the first few Fourier components of the oscillation in Figure 2.12. More generally the shape of the oscillation is determined, say, by the amplitude ratios a_k/a_1 and the phase differences $\phi_k - k\phi_1$. These quantities have proved very convenient for the characterization of observed light curves (*e.g.* Andreasen & Petersen 1987), as well as for the analysis of numerical results. One may hope that further work in this direction will allow an understanding of the physical reasons underlying the observed behaviour.

In a double-mode, large-amplitude pulsating star, with basic frequencies ω_1 and ω_2 , Fourier analysis in general produces peaks at the combination frequencies $k\omega_1 + j\omega_2$, for integral k and j . Thus the spectrum may become quite complex. In particular, the detection of additional basic frequencies is difficult, since these might easily be confused with the combination frequencies, given the finite observational resolution.

2.3 Results on solar oscillations

By far the richest spectrum of oscillations has been observed for the Sun; this allows detailed investigations of the properties of the solar interior. Thus it is reasonable to summarize the observational situation for the Sun. Figure 2.13 shows schematically the modes that have been definitely observed, as well as modes for which detection has been claimed in the past. Only the modes in the five-minute region have definitely been observed and identified. As mentioned in Chapter 1, they are standing acoustic waves, generally of high radial order. It is interesting that they are observed at all values of the degree, from purely radial modes at $l = 0$ to modes of very short horizontal wavelength at $l = 1500$. Furthermore, there is relatively little change in the amplitude per mode between these two extremes. The p and f modes have now been detected to frequencies as low as $500 \mu\text{Hz}$ (*e.g.* Schou 1998; Bertello *et al.* 2000). The apparent existence of oscillations at even lower frequency has caused very substantial interest; if real and of solar origin, they would correspond to standing gravity waves, or g modes, whose frequencies are very sensitive to conditions in the deep solar interior. However, it should be noted that recent analyses have provided stringent upper limits to the amplitudes of such modes, which makes highly questionable earlier claims of detections (*e.g.* Appourchaux *et al.* 2000).

Figure 2.14 shows an example of an observed power spectrum of solar oscillations. This was obtained by means of Doppler velocity measurements in light integrated over the solar disk, and hence, according to the analysis in Section 2.1, is dominated by modes of degrees 0 – 3. The data were obtained from the BiSON network of six stations globally distributed in longitude, to suppress the daily side-bands, and span roughly four months. Thus the intrinsic frequency resolution, as determined by equation (2.25), is smaller than the thickness of the lines. There is a visible increase in the line-width when going from low to high frequency. The broadening of the peaks at high frequency is probably caused by the damping and excitation processes, as discussed in Section 2.2.4; thus the observations indicate that the damping rate increases with increasing frequency. Finally, there is clearly

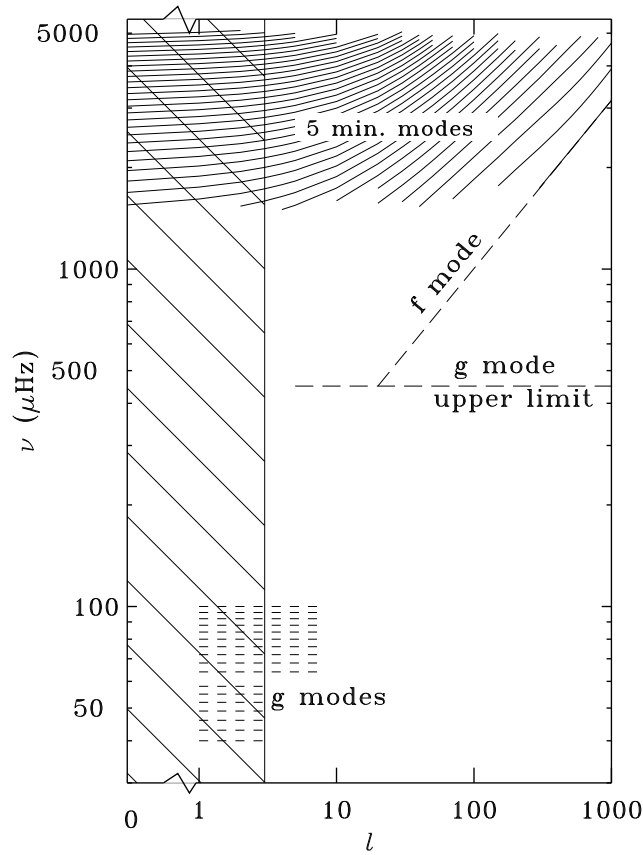


Figure 2.13: Schematic illustration of the oscillations observed in the Sun. The 5 minute oscillations are standing acoustic waves. They have been completely identified. Each of the lines in this part of the diagram corresponds to a given value of the radial order n . The f mode, which is essentially a surface gravity wave, has been observed at high degree; acoustic modes have frequencies exceeding that of the f mode. The presence of the long-period oscillations was suggested by early observations, but the reality, let alone solar origin, of these oscillations has not been established; had they corresponded to oscillations of the Sun, they would likely have been g modes of low degree. Note that g modes are restricted to lie underneath the frequency indicated as “g mode upper limit”. The hatching indicates the region in l that can be observed in light integrated over the disk, as is generally the case for stars.

a well-defined distribution of amplitudes, with a maximum around 3000 μHz and very small values below 2000, and above 4500, μHz . The maximum power corresponds to a velocity amplitude of around 15 cm s^{-1} ; observations in broad-band intensity show amplitudes up to around 4 ppm. The power distribution is essentially the same at all degrees where the five-minute oscillations are observed. An interesting analysis of the observed dependence of

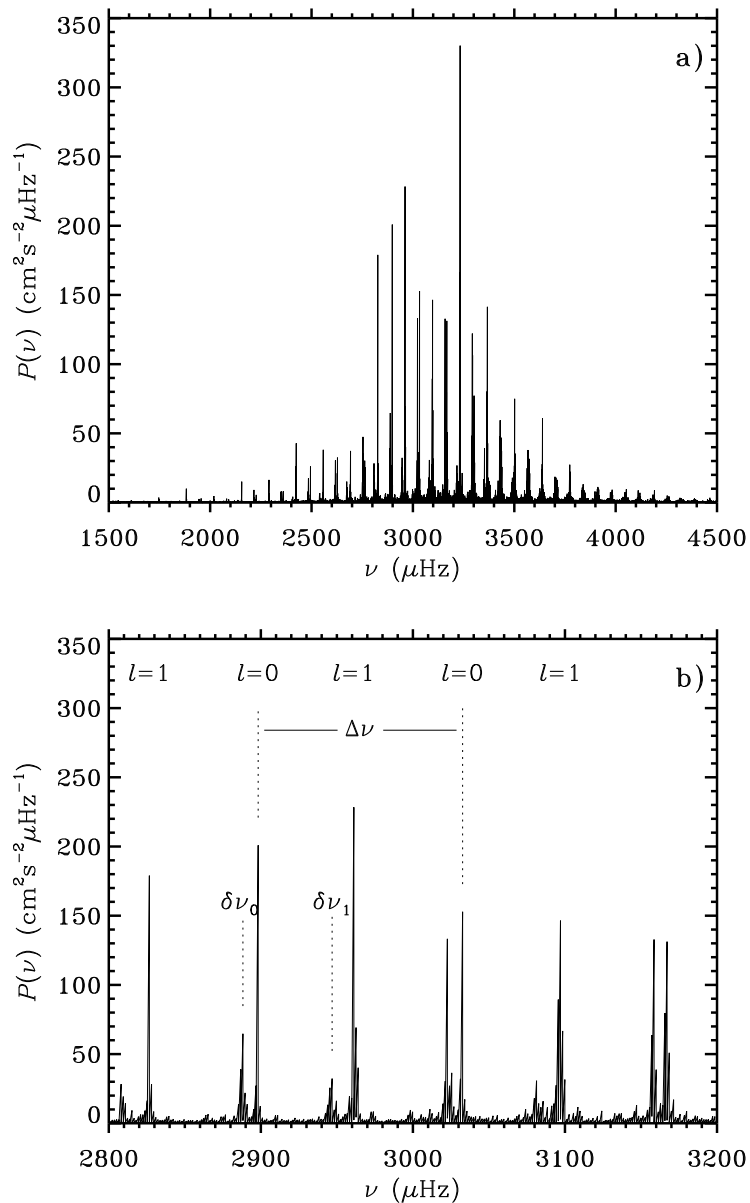


Figure 2.14: Power spectrum of solar oscillations, obtained from Doppler observations in light integrated over the disk of the Sun. The ordinate is normalized to show velocity power per frequency bin. The data were obtained from six observing stations and span approximately four months. Panel (b) provides an expanded view of the central part of the frequency range. Here some modes have been labelled by their degree l , and the large and small frequency separations $\Delta\nu$ and $\delta\nu_l$ [*cf.* equations (2.40) and (2.41)] have been indicated. (See Elsworth *et al.* 1995.)

mode amplitudes on degree, azimuthal order and frequency was presented by Libbrecht *et al.* (1986). Woodard *et al.* (2001) recently made a careful investigation of the dependence of the mode energy on degree and frequency of oscillation, based on observations from the SOHO spacecraft.

The spectrum illustrated in Figure 2.14 evidently has a highly regular frequency structure, most clearly visible in the expanded view in panel (b). This reflects the asymptotic expression in equation (2.32), apart from the rotational effects which are invisible at this frequency resolution. According to the leading term in equation (2.32), the peaks should occur in groups corresponding to even and odd degree, such that $n + l/2$ are the same, the groups being uniformly spaced with a separation $\Delta\nu/2$; this apparent degeneracy is lifted by the second term in equation (2.32). Thus the spectrum is characterized by the *large frequency separation*

$$\Delta\nu = \nu_{n+1l} - \nu_{nl} , \quad (2.40)$$

and the *small frequency separation*

$$\delta\nu_l = \nu_{nl} - \nu_{n-1l+2} \simeq (4l + 6)D_0 . \quad (2.41)$$

These separations are indicated in Figure 2.14b, where also selected peaks corresponding to $l = 0$ and 1 have been labelled, in each case with a neighbouring peak with $l = 2$ or 3, respectively. It should be noticed that the observed amplitudes of the $l = 3$ peaks are much reduced relative to the $l = 1$ peaks, as predicted by the spatial response function $S_l^{(V)}$ shown in Figure 2.2; on the other hand, the observed amplitudes for $l = 0$ and 2 are roughly similar, as expected.

To illustrate in more detail the properties of the frequency spectrum, it is convenient to use an *echelle diagram* (*e.g.* Grec, Fossat & Pomerantz 1983). Here the frequencies are reduced modulo $\Delta\nu$ by expressing them as

$$\nu_{nl} = \nu_0 + k\Delta\nu + \tilde{\nu}_{nl} , \quad (2.42)$$

where ν_0 is a suitably chosen reference, and k is an integer such that $\tilde{\nu}_{nl}$ is between 0 and $\Delta\nu$; the diagram is produced by plotting $\tilde{\nu}_{nl}$ on the abscissa and $\nu_0 + k\Delta\nu$ on the ordinate. Graphically, this may be thought of as cutting the frequency axis into pieces of length $\Delta\nu$ and stacking them above each other. If the asymptotic relation (2.32) had been precisely satisfied, the result would be points arranged on a set of vertical lines corresponding to the different values of l , the lines being separated by the appropriate $\delta\nu_l$. The actual behaviour is shown in Figure 2.15, based on frequencies from BiSON observations. The general behaviour is clearly as expected, although with significant departures. The curvature of the lines indicate that the frequency for each l are not precisely uniformly spaced; as discussed in Section 7.7.3 this results from variations in structure near the solar surface. Also, it is fairly evident that the small separation varies with mode order.

To illustrate the quality of current frequency determinations, Figure 2.16 shows observed frequencies at low and moderate degree from one year's observations with the High Altitude Observatory's LOWL instrument (see Tomczyk *et al.* 1995). The error bars have been magnified by a factor 1000 over the usual 1σ error bars. For the most accurate measurements, the relative standard deviation is well below 10^{-5} , thus substantially exceeding the precision with which the solar mass is known. Precise measurements of frequencies, frequency separations and rotational splittings for low-degree modes were published by Elsworth *et al.* (1990), Toutain & Fröhlich (1992), Fröhlich *et al.* (1997), Lazrek *et al.* (1997), Chaplin

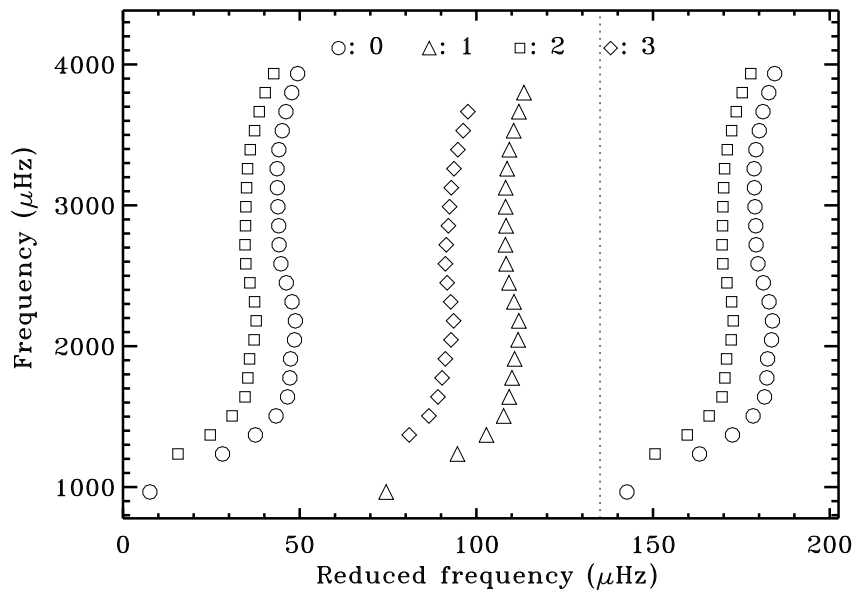


Figure 2.15: Echelle diagram for observed solar frequencies obtained with the BiSON network (Chaplin *et al.* 2002), plotted with $\nu_0 = 830 \mu\text{Hz}$ and $\Delta\nu = 135 \mu\text{Hz}$ (*cf.* eq. 2.42). Circles, triangles, squares and diamonds are used for modes of degree $l = 0, 1, 2$ and 3 , respectively. For clarity the points for $l = 0$ and 2 have been repeated in the right-hand part of the diagram; the dotted vertical line indicates $\Delta\nu$.

et al. (1998, 1999, 2001ab); such measurements are of great diagnostic importance for the properties of the solar core (*cf.* Section 7.3). An extensive set of high-degree frequencies was obtained by Bachmann *et al.* (1995).

From spatially resolved observations, individual frequencies ω_{nlm} can in principle be determined. Because of observational errors and the large amount of data resulting from such determination, it has been common to present the results in terms of coefficients in fits to the m -dependence of the frequencies, either averaged over n at given l (Brown & Morrow 1987) or for individual n and l (*e.g.*, Libbrecht 1989). A convenient form of the expansion was established by Ritzwoller & Lavelly (1991); this can be expressed as

$$\omega_{nlm} = \omega_{nl0} + 2\pi \sum_{j=1}^{j_{\max}} a_j(n, l) \mathcal{P}_j^{(l)}(m), \quad (2.43)$$

in terms of the so-called a coefficients $a_j(n, l)$. Here the $\mathcal{P}_j^{(l)}$ are polynomials of degree j which satisfy the orthogonality relation $\sum_m \mathcal{P}_i^{(l)}(m) \mathcal{P}_j^{(l)}(m) = 0$ for $i \neq j$ (see also Schou *et al.*, 1994). Explicit expressions for these polynomials were given by Pijpers (1997). As discussed in Chapters 8 and 9 [*cf.* Section 8.2 and equation (9.25)] the coefficients a_j with odd j arise from rotational splitting; the coefficients with even j are caused by departures

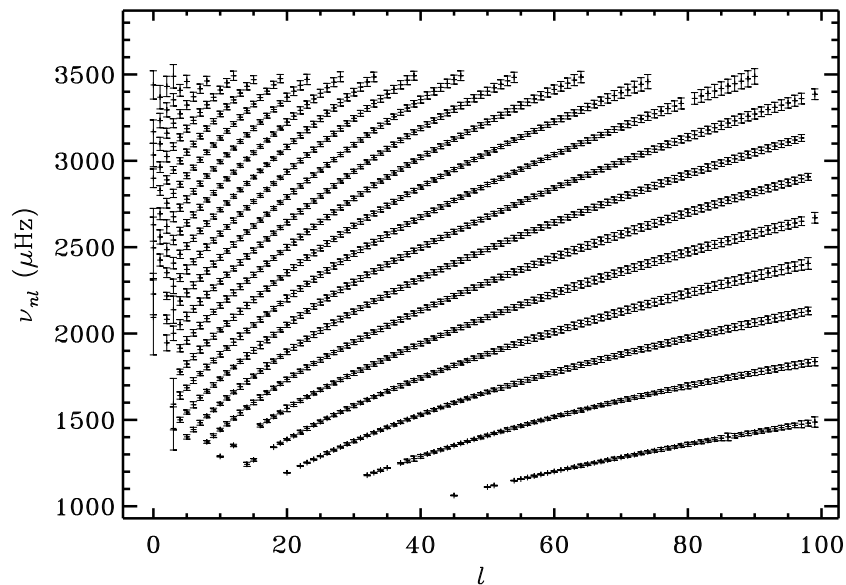


Figure 2.16: Plot of observed solar p-mode multiplet frequencies, as a function of the degree l , from one year of observations. The vertical lines show the 1000σ error bars. Each ridge corresponds to a given value of the radial order n , the lowest ridge having $n = 1$. (See Tomczyk, Schou & Thompson 1996).

from spherical symmetry in solar structure, or from effects of magnetic fields.

It is probably a fair assessment that the major developments in helioseismology in recent years have resulted from improvements in the observations. The principal problems in early data was the presence of gaps, leading to sidebands in the power spectra, and the effects of atmospheric noise. The problems with gaps have been overcome through observations from global networks; nearly continuous observations, which are furthermore free of effects of the Earth's atmosphere, have been obtained from space. The result has been greatly sets of frequencies, extending to high degree, which has very substantially improved our knowledge about the solar interior.

As shown in Figure 2.9, gaps in the timeseries introduce sidebands in the spectrum; these add confusion to the mode identification and contribute to the background of noise in the spectra. Largely uninterrupted timeseries of several days', and up to a few weeks', duration have been obtained from the South Pole (*e.g.* Grec *et al.* 1980; Duvall *et al.* 1991); however, to utilize fully the phase stability of the modes at relatively low frequency requires continuous observations over far longer periods, and these cannot be obtained from a single terrestrial site.

Nearly continuous observations can be achieved from a network of observing stations, suitably placed around the Earth (*e.g.* Hill & Newkirk 1985). An overview of network projects was given by Hill (1990). A group from the University of Birmingham has operated

the BiSON¹ network for many years, to perform whole-disk observations using the resonant scattering technique (*e.g.* Chaplin *et al.* 1996). A similar network (the IRIS² network) has been set up by a group at the University of Nice (Fossat 1991).

An even more ambitious network has been established in the GONG³ project, organized by the National Solar Observatory of the United States (for introductions to the project, see Harvey, Kennedy & Leibacher 1987; Harvey *et al.* 1996). This project has involved the setting up at carefully selected locations of six identical observing stations. They use an interferometric technique to observe solar oscillations of degrees up to around 250. In addition to the design and construction of the observing equipment, a great deal of effort is going into preparing for the merging and analysis of the very large amounts of data expected, and into establishing the necessary theoretical tools. The network became operational in October 1995 when the last station, in Udaipur (India) started observing. The GONG network, and early results obtained with it, was described by Gough *et al.* (1996) and in accompanying papers.

Major efforts have gone into the development of helioseismic instruments for the *SOHO*⁴ spacecraft, which was launched in December 1995 (*e.g.* Domingo, Fleck & Poland 1995), as a joint project between ESA and NASA. *SOHO* is located near the L₁ point between the Earth and the Sun, and hence is in continuous sunlight. This permits nearly unbroken observations of solar oscillations. A further advantage is the absence of effects from the Earth's atmosphere. These are particularly troublesome for observations of high-degree modes, where seeing is a serious limitation (*e.g.* Hill *et al.* 1991), and for intensity observations of low-degree modes, which suffer from transparency fluctuations.

SOHO carries three instrument packages for helioseismic observations:

- The GOLF instrument (for **G**lobal **O**scillations at **L**ow **F**requency; see Gabriel *et al.* 1995, 1997). This uses the resonant scattering technique in integrated light. Because of the great stability of this technique, it is hoped to measure oscillations at comparatively low frequency, possibly even g modes. Unlike the p modes, which have formed the basis for helioseismology so far, the g modes have their largest amplitude near the solar centre; hence, detection of these modes would greatly aid the study of the structure and rotation of the core. Also, since the lifetime of p modes increases rapidly with decreasing frequency, very great precision is possible for low-frequency p modes.
- The SOI-MDI experiment (for **S**olar **O**scillations **I**nvestigation – **M**ichelson **D**oppler **I**mager; see Scherrer *et al.* 1995; Rhodes *et al.* 1997) uses the Michelson interferometer technique. By observing the entire solar disk with a resolution of 4 arcseconds, and parts of the disk with a resolution of 1.2 arcseconds, it is possible to measure oscillations of degree as high as a few thousand; furthermore, very precise data have been obtained on modes of degree up to about 1000, including those modes for which ground-based observation is severely limited by seeing. As a result, it has been possible to study the structure and dynamics of the solar convection zone, and of the radiative interior, in great detail.

¹Birmingham Solar Oscillation Network

²International Research on the Interior of the Sun

³Global Oscillation Network Group

⁴Solar and Heliospheric Observatory

- The VIRGO experiment (for **V**ariability of solar **I**rradiance and **G**ravty **O**scillations; see Fröhlich *et al.* 1995, 1997). This contains radiometers and Sun photometers to measure oscillations in solar irradiance and broad-band intensity. It is hoped that this will allow the detection of g modes; furthermore, the observations supplement those obtained in Doppler velocity, particularly with regards to investigating the phase relations for the oscillations in the solar atmosphere.

Several very extensive tables of five-minute oscillation frequencies have become available in recent years. As examples, tables of multiplet frequencies are provided at <http://astro.phys.au.dk/~jcd/oscilnotes/data/>. One set, described in more detail by Basu *et al.* (1997), consists of a combination of BiSON low-degree data and data for modes of low and intermediate degree from the LOWL instrument. The second set was obtained from around 4 months of observations with the GONG network (see Schou *et al.* 2002). Links to further data are also given; these in particular include very extensive results obtained with the MDI instrument on SOHO, covering both multiplet frequencies and a coefficients (*cf.* eq. 2.43) (see Schou 1999; Schou *et al.* 2002).

2.4 Other types of multi-periodic stars

Observations of stellar oscillations provide constraints on the properties of the star and, as mentioned in Chapter 1, the information content increases with the number of observable modes. Fortunately, pulsating stars are found throughout the Hertzsprung-Russell diagram. This is illustrated schematically in Fig. 2.17, which summarizes the known classes of stars, in relation to selected evolution tracks; some of these classes will be discussed in more detail in the following,

An important region in the diagram is the *Cepheid instability strip*, populated by the Cepheids ('Ceph') and RR Lyrae stars ('RR Lyr') as well as, close to the main sequence, the δ Scuti stars (' δ Sct'). These are believed to be excited by an opacity mechanism associated with the second helium ionization zone; as discussed in detail in Chapter 10 this provides an explanation for the localized nature of these stars in the HR diagram. In the Cepheids and RR Lyrae stars typically only a single period is observed, in most cases assumed to correspond to the fundamental radial mode. The stars near the main sequence, on the other hand, generally show several periods, making them potentially more interesting for investigations of the stellar interiors. This is also true for the more massive slowly pulsating B stars ('SPB') and β Cephei stars (' β Cep'); the former have periods of around a day or more whereas the latter have periods of the order of hours. These oscillations are also excited by opacity mechanisms, although related to opacity features dominated by iron-group elements.

The rapidly oscillating Ap stars ('roAp') are also located in the instability strip, but with fairly peculiar characteristics. They oscillate in high-order acoustic modes, rather like the Sun, but the oscillations are closely tied to the large-scale magnetic field found in these stars; this is probably related to the abundance inhomogeneities set up across the stellar surface as a result of the suppression of convection by the magnetic field.

Red giants show oscillations of very long periods, corresponding to the large dynamic timescale resulting from their huge radii (*cf.* eq. 1.1). The Mira variables have very large amplitudes in the visible band, up to eight magnitudes, although the amplitude in the luminosity oscillations are more modest; much of the effect in the visible arises from the

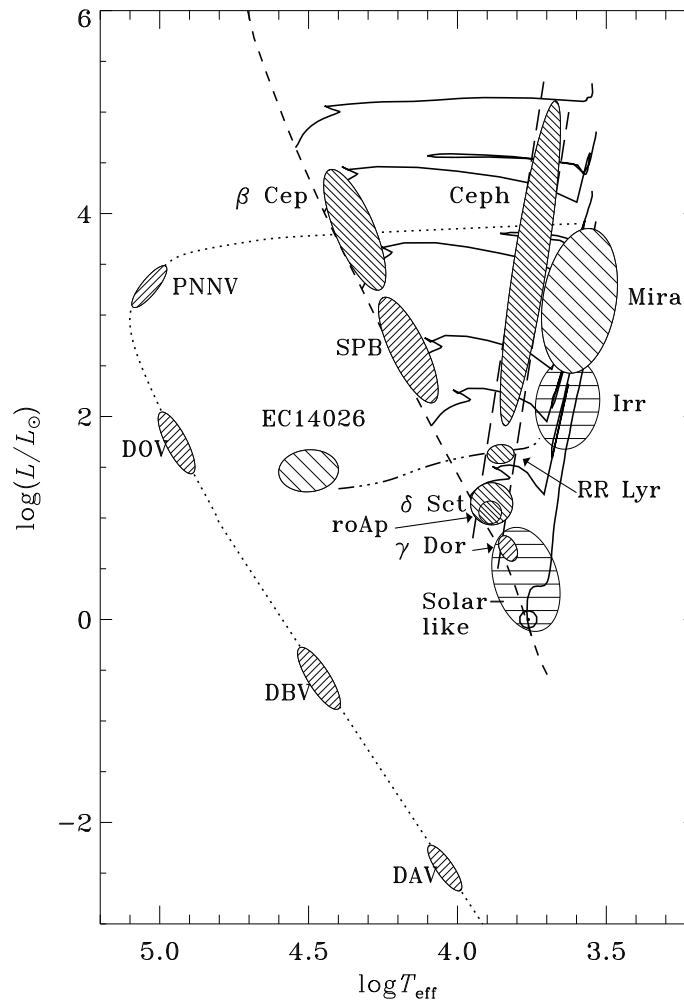


Figure 2.17: Schematic Hertzsprung-Russell diagram illustrating the location of several classes of pulsating stars. The dashed line shows the zero-age main sequence, the continuous curves are selected evolution tracks, at masses 1, 2, 3, 4, 7, 12 and $20 M_{\odot}$, the dot-dashed line is the horizontal branch and the dotted curve is the white-dwarf cooling curve.

temperature-sensitivity of the formation of molecules in the stellar atmospheres. They are typically single periodic. The irregular variables ('Irr') have lower amplitudes and show variations in the amplitudes and possibly periods.

The final stages of stellar evolution are represented by the subdwarf B variable stars (also known as 'EC 14026' stars, after the first member of the group to be discovered), discussed in more detail in Section 2.4.3 below. Their pulsations are also, as for the main-sequence B stars, caused by an opacity mechanism related to iron-group elements. Several groups of white dwarfs, discussed in Section 2.4.4, also pulsate.

Finally, oscillations corresponding to those observed in the Sun are expected in a broad group of stars. The solar oscillations are believed to be excited stochastically by the near-surface convection (see also Section 10.6). Thus oscillations of a similar nature are expected in all stars with effective temperature $T_{\text{eff}} \lesssim 7000$ K, which have vigorous outer convection. As discussed in Section 2.4.1, this expectation has recently been dramatically confirmed.

2.4.1 Solar-like oscillations in other stars

The archetypal example is obviously the spectrum shown in Figure 2.14, obtained for the Sun observed as a star, in disk-averaged light. This is characterized by a broad spectrum of almost uniformly spaced peaks, approximately satisfying the asymptotic relation (2.32) and hence characterized by the large frequency separation $\Delta\nu$ and the small frequency separation $\delta\nu$ [*cf.* equations (2.40) and (2.41)]. The power distribution results from the broad-band nature of the excitation (see also Section 10.6) which causes all modes in a fairly extensive frequency range to be excited. This greatly simplifies the identification of the modes and hence the comparison with stellar models. In the search for solar-like oscillations the nearly uniformly spaced frequency pattern, and the distribution of mode power, are typically the characteristics to look for.

The main difficulty in observing solar-like oscillations are the extremely small amplitudes, either in Doppler or intensity observations, judging from the maximal solar amplitudes of around 15 cm s^{-1} and 4 ppm, respectively. Christensen-Dalsgaard & Frandsen (1983a) made rough estimates of the expected amplitudes from which Kjeldsen & Bedding (1995) concluded that the amplitudes approximately scaled proportional to

$$\frac{L}{M} \propto \frac{T_{\text{eff}}^4}{g_s}, \quad (2.44)$$

where L and M are the luminosity and mass of the star, and g_s is the surface gravity. More detailed calculations by Houdek *et al.* (1999) largely confirmed these results (see also Section 10.3). Accordingly, main-sequence stars more massive than the Sun are expected to have substantially higher amplitudes, and relatively large amplitude are predicted for red giants.

A major improvement in the observational techniques has recently resulted from the development of very stable radial-velocity measurements to search for extra-solar planets as reflected in the motion of their central stars. As discussed below, these have led to striking detections of solar-like oscillations in a few cases, and more detections and detailed investigations are expected in the near future from such observations.

Very substantial observational efforts have been made to detect solar-like oscillations in stars near the main sequence. For example, Gilliland *et al.* (1993) carried out an extensive coordinated campaign on the open cluster M67, with most of the world's largest telescopes; this failed to detect any oscillations, in some cases with upper limits well below the theoretical predictions. Perhaps the first plausible detection was made by Kjeldsen *et al.* (1995), who observed the subgiant η Bootis using a technique based on measurements of equivalent widths of spectral lines. The resulting power spectrum, shown in Figure 2.18, does display the enhancement of power expected for solar-like oscillations; the determination of the oscillation frequencies was complicated by the fact that only observations from a single site were observable, leading to the window function (*cf.* Section 2.2.3) illustrated in the inset. However, Kjeldsen *et al.* were able to determine both the frequency separations $\Delta\nu$

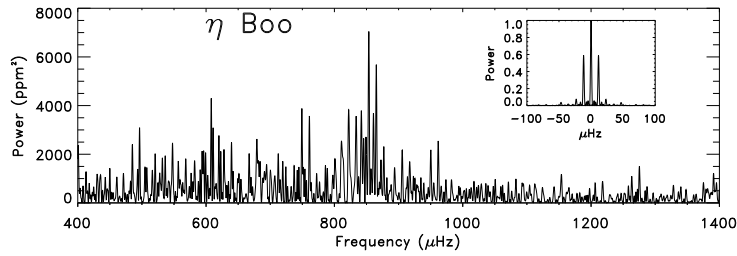


Figure 2.18: Observed power spectrum of η Bootis, based on equivalent-width observations by Kjeldsen *et al.* (1995). The inset shows the window function of these single-site observations. (From Bedding & Kjeldsen 1995.)

and $\delta\nu_0$, which were in reasonable agreement with expectations based on evolution models of the star. It should be noted, however, that Brown *et al.* (1997) failed to find oscillations in this star in Doppler velocity, with an upper limit which they estimated to be well below the amplitudes claimed by Kjeldsen *et al.*; thus the reality of these oscillations remains somewhat questionable.

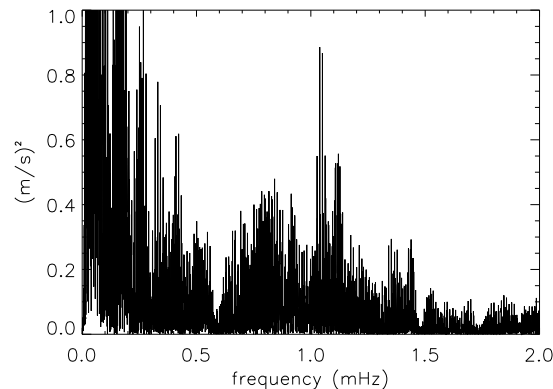


Figure 2.19: Observed power spectrum of Procyon, based on radial-velocity observations. (From Barban *et al.* 1999.)

A promising case is Procyon (α CMi) where Brown *et al.* (1991) reported oscillations in radial velocity with approximately the expected dependence on frequency. This early detection has recently been confirmed by Martić *et al.* (1999), again using radial-velocity observations; a power spectrum of these observations is shown in Figure 2.19. A careful analysis by Barban *et al.* (1999), comparing the observed spectra with simulated data for models of Procyon, led to a determination of the large separation $\Delta\nu \simeq 56 \mu\text{Hz}$, in good agreement with model predictions. Interestingly, the observed amplitude was only about

1/3 of the predictions, confirming the inference from M67 that the theoretical estimates provide an overestimate; it should be noted that both Procyon and the stars observed in M67 are somewhat hotter than the Sun.

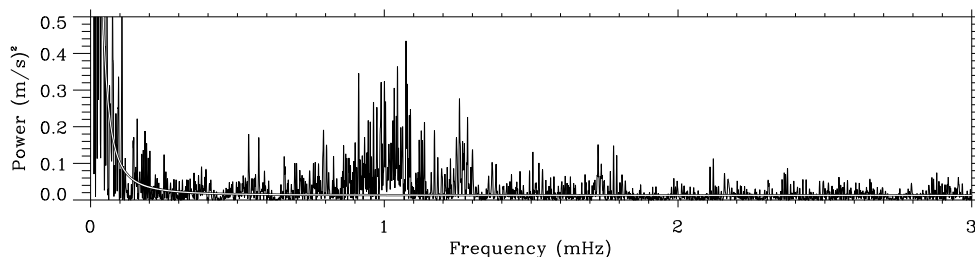


Figure 2.20: Power spectrum of β Hydri, from radial-velocity observations by Bedding *et al.* (2001). The white line marks the noise level.

Detection of a power enhancement at the expected frequency was recently reported by Bedding *et al.* (2001) from radial-velocity observations of the star β Hyi. This is a subgiant with approximately the same effective temperature as the Sun, while the luminosity is higher by a factor of around 3.5. The resulting power spectrum is shown in Figure 2.20; there is a very clearly defined enhancement of power around 1 mHz, far exceeding the noise level. This is perhaps the first incontrovertible detection of solar-like oscillations in another star; the amplitude is approximately consistent with theoretical expectations.

A star of particularly great interest is α Cen A: it is quite similar to the Sun and, being member of a nearby well-studied binary system, its parameters are known quite precisely. Detailed modelling of the α Cen system has been carried out by Guenther & Demarque (2000) and Morel *et al.* (2000). Kjeldsen *et al.* (1999) carried out extensive observations of line-intensity variations in α Cen A; although hints of oscillations were found, they were only able definitely to determine an upper limit to the oscillations, consistent with expectations. Very encouraging results have been obtained using the star tracker on the otherwise failed WIRE satellite (see Buzasi 2000). Schou & Buzasi (2001) obtained a convincing detection of oscillations in continuum intensity, with a maximum amplitude of around 6 ppm, roughly consistent with theoretical expectations and a large separation of $106 \mu\text{Hz}$, again largely consistent with model predictions. Definite Doppler-velocity observations, with a remarkable signal-to-noise ratio, were obtained by Bouchy & Carrier (2001) with the Swiss CORALIE instrument⁵ on La Silla. The resulting power spectrum, shown in Figure 2.21, has a power distribution similar to what is observed in the Sun, although shifted to slightly lower frequency. A substantial number of modes have been identified in the spectrum, although at the time of writing these have not yet been definitely identified. As in the other cases a serious difficulty with the analysis is the fact that the observations shown in Figure 2.21 are from a single site; however, simultaneous observations from the Anglo-Australian Telescope in Australia are currently being analyzed and will likely help substantially in reducing the sidebands in the spectrum. These results show the power of modern carefully stabilized spectrographs for this type of observations. Even more dramatic results can be

⁵developed to search for extra-solar planets by measuring the resulting radial velocity of the central stars

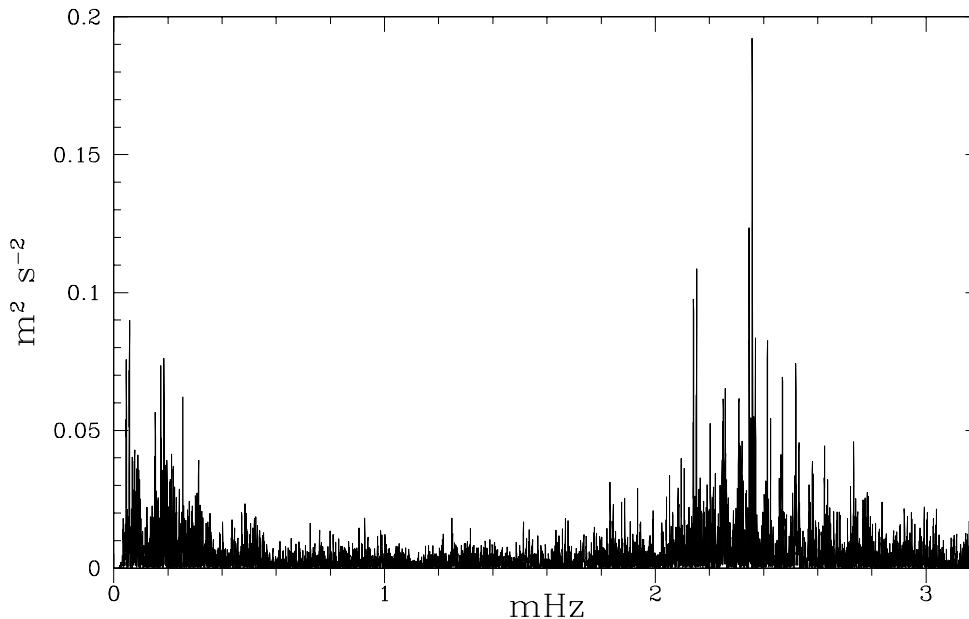


Figure 2.21: Power spectrum of oscillations of α Cen A, from radial-velocity observations with the CORALIE spectrograph. (From Bouchy & Carrier 2001.)

expected when the HARPS instrument starts operations on the ESO 3.6-m telescope on La Silla.

As mentioned above, solar-like oscillations of relatively large amplitude may be expected in red giants. Strong evidence has been found for solar-like oscillations in the star Arcturus (*e.g.* Smith, McMillan & Merline 1987; Innis *et al.* 1988; Merline 1998), including indications of a frequency pattern in accordance with the dominant behaviour of equation (2.32). Also, Edmonds & Gilliland (1996) found variations in K giants in the globular cluster 47 Tuc which were apparently consistent with solar-like pulsations. Based on observations with the WIRE star tracker Buzasi *et al.* (2000) claimed detection of solar-like oscillations in α Ursa Majoris A, a giant of spectral type K0 III, with an estimated mass, from membership of a binary system, of around $5M_{\odot}$. Guenther *et al.* (2000) analyzed the evolution and oscillation frequencies of this star. They noted that, as a result of the late evolutionary state of the star, the spectra for $l > 0$ were completely dominated by modes behaving like g modes, leading to very dense frequency spectra; thus the only modes that could realistically be identified were the radial modes, which are purely acoustic. Comparing with the observed frequencies, they obtained a tentative identification of some of the modes, although they noted that this was not yet unique. Dziembowski *et al.* (2001) carried out a more careful analysis of the possible causes of oscillations of α UMa A and concluded that the observed properties of the amplitudes were unlikely to be consistent with solar-like, stochastic excitation. Thus the current results on α UMa should perhaps be regarded with some caution.

Even so, red giants remain promising targets for asteroseismology. Frandsen *et al.*

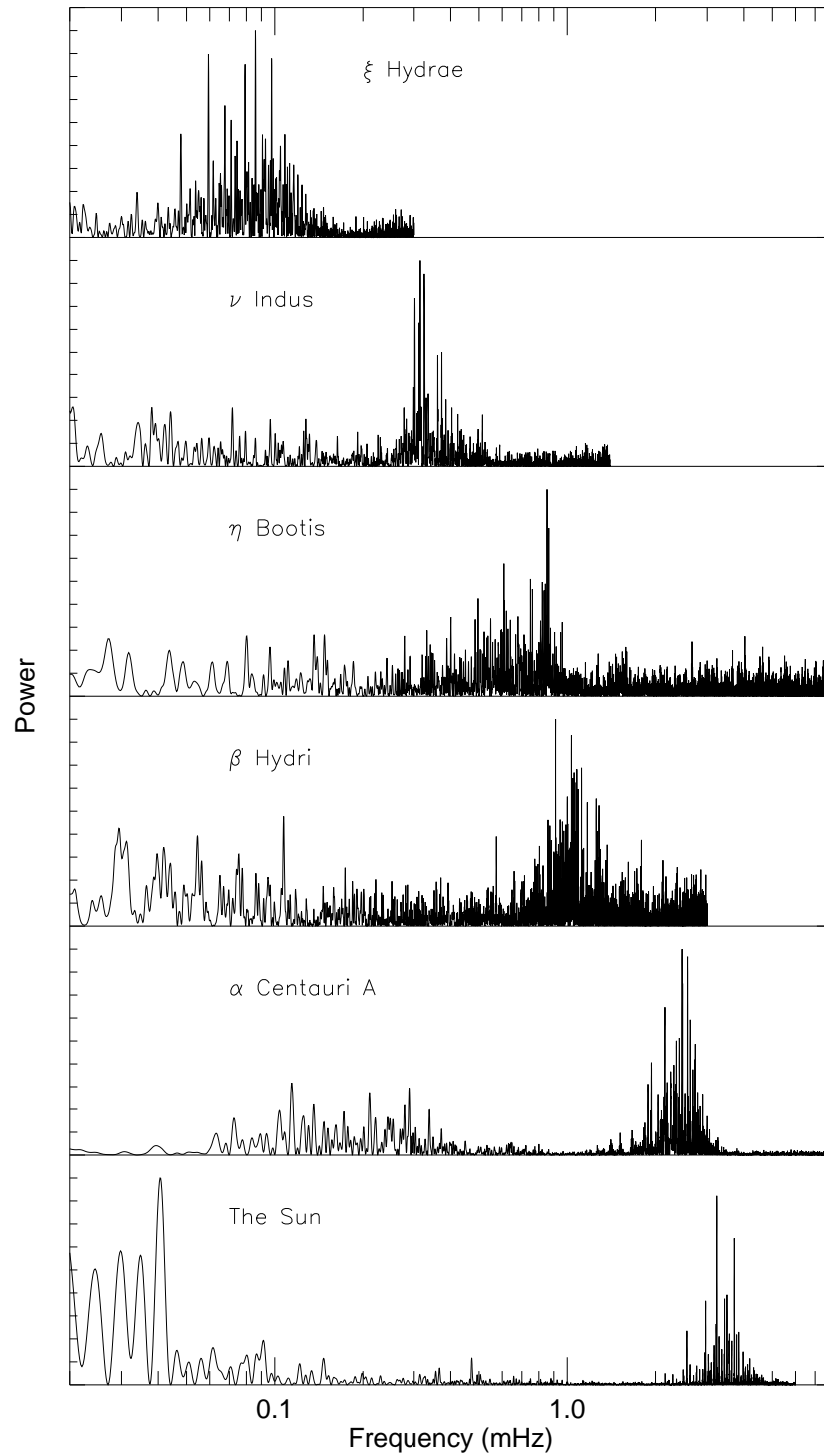


Figure 2.22: Power spectra of 5 stars showing solar-like oscillations, compared with solar data from the GOLF instrument. The power scale is arbitrary. (Figure kindly provided by Hans Kjeldsen.)

(2002) obtained clear evidence for solar-like oscillations in ξ Hydrae, using the CORALIE instrument. This star is in the shell hydrogen-burning, or perhaps more likely in the core helium-burning, stage (see also Teixeira *et al.* 2003). With a radius of $10R_{\odot}$ and a mass of $3M_{\odot}$, the maximum power is at periods of around 3 – 4 hours; but the power distribution is otherwise quite similar to the solar case.

An overview of some of the stars for which solar-like oscillations have been observed is provided by Figure 2.22, based largely on data obtained by the Aarhus and Sydney groups. Here solar data from the GOLF instrument are included, analyzed over a period of 55 hours, to provide a frequency resolution corresponding approximately to the data for α Cen A. The similarity of the power distributions, over a large range in stellar parameters and hence frequencies, is obvious.

For red supergiants the relevant periods are of order weeks or months, and hence decades of observations are required to resolve the oscillations and study their properties. Fortunately, very extensive sets of data are available from amateur observations, spanning in some cases a century. Although the precision of these mostly visual estimates is not as high as for professional observations, the large amplitudes of the variability allow reliable analysis of the oscillations; also the very extensive base of observations makes it possible to study the statistical properties of the variability. In a very interesting analysis, Mattei *et al.* (1997) related the *variability* in the oscillation amplitudes to the amplitudes. This isolated the semi-regular variables as a clearly defined class, with a strong correlation between variability and amplitude. Christensen-Dalsgaard, Kjeldsen & Mattei (2001) argued that this relation corresponded closely to what would result from stochastically excited oscillations where the amplitudes have an exponential distribution, as has indeed been verified for the Sun (*e.g.* Kumar, Franklin & Goldreich 1988; Chaplin *et al.* 1997; Chang & Gough 1998; see also Section 10.3). Also, Bedding (2003) analyzed several examples of long-period variables, obtaining oscillation spectra reminiscent of solar-like oscillations. If confirmed by more detailed analyses, such studies would provide extensive data on the excitation of solar-like oscillations over a very broad range of stellar parameters.

The increasing observational basis for the study of solar-like oscillations in other stars evidently promises extremely valuable information about the interior properties of these stars and hence tests of the theory of stellar structure and evolution. In addition, the results provide information about the excitation mechanisms responsible for the oscillations. From the unexpectedly low amplitude found in Procyon, and the low upper limit to detections in M67, it is already clear that the scaling in equation (2.44) predicts too high amplitudes for stars hotter than the Sun. Interestingly, the amplitudes observed so far appear rather to be consistent with a scaling with g_s^{-1} (evidently, for stars with effective temperature close to the that of Sun such as η Boo, α Cen A or β Hyi, the two scalings are equivalent). The physical reason for this behaviour is so far not understood.

2.4.2 Observations of δ Scuti oscillations

The δ Scuti stars fall in an extension of the Cepheid instability strip, close to the main sequence. They typically have masses around 2 – $2.5M_{\odot}$ and are either near or just after the end of core hydrogen burning. Although they have been recognized as a separate class of pulsating stars since the work of Eggen (1957ab), only within the last decade have the details of their spectra of pulsations become clear. The fact that these stars typically have periods of the order of one hour presents a considerable difficulty: observations from

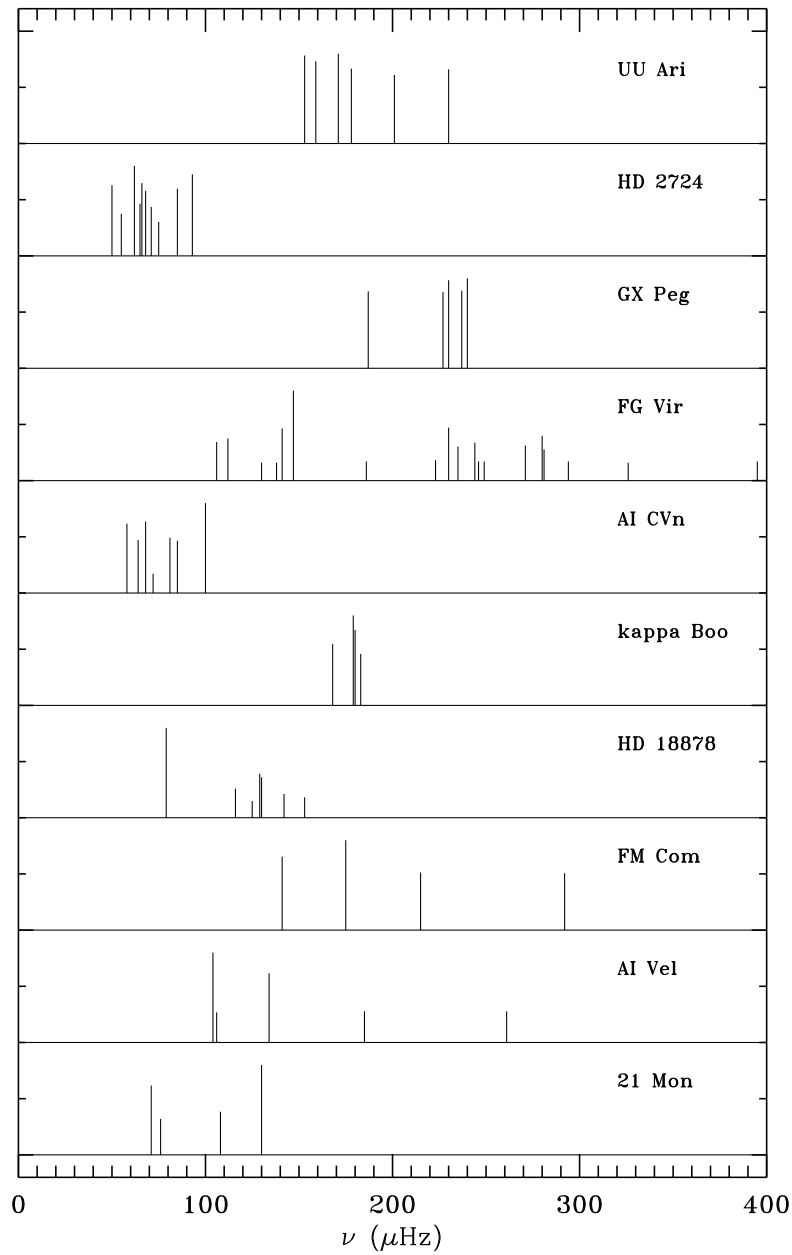


Figure 2.23: Schematic oscillation spectra of a number of δ Scuti stars.

a single site will lead to a great deal of confusion from the side-bands (*cf.* Section 2.2.3), complicating the determination of the oscillation frequencies. However, thanks to a number of observing campaigns involving two or more observatories extensive data for a number of stars have become available (*e.g.* Michel & Baglin 1991; Michel *et al.* 1992; for reviews, see Breger 1995ab). A detailed discussion of many aspects of the study of δ Scuti stars was

provided in the volume edited by Breger & Montgomery (2000).

The most extensive observations of δ Scuti stars have been photometric, although the oscillations have also been observed spectroscopically. Recent multi-site campaigns have resulted in the determination of very substantial sets of frequencies in some cases (*e.g.* Breger *et al.* 1998, 1999; Handler *et al.* 2000). Schematic spectra of several stars are shown in Figure 2.23. The observed frequency range corresponds to low-order acoustic modes. However, the distributions of modes excited to observable frequencies are evidently strikingly different: in some cases only modes in a narrow frequency band are found, whereas in other cases the observed modes extend quite widely in frequency. So far, no obvious correlation between the frequency distribution and other parameters of the stars has been found.

From a comparison with computed oscillation spectra (see Section 5.3.2) it is clear that only a subset of the possible modes of oscillation are excited to observable amplitudes in these stars. However, the reasons for the mode selection is currently unclear. This greatly complicates the mode identification. A further complication comes from the fact that the basic parameters of these stars, such as their mass and radius, are in most cases known with poor accuracy. On the other hand, the δ Scuti stars have the potential for providing very valuable information about stellar evolution: unlike the Sun, these stars have convective cores, and hence the frequency observations may give information about the properties of such cores, including the otherwise highly uncertain degree of overshoot from the cores. Therefore, a great deal of effort is going into further observations of δ Scuti stars as well as in calculations to elucidate the diagnostic potential of the observations and analyze the existing data. Particularly promising are observations of δ Scuti stars in open clusters. With CCD photometry it is possible to study several variable stars in such a cluster at once, and furthermore “classical” observations of the cluster can be used to constrain the parameters of the stars, such as their distance, age and chemical composition (*e.g.* Breger *et al.* 1993ab; Hernández *et al.* 1998).

2.4.3 Subdwarf B variables

This group of stars⁶ was identified as pulsating in parallel theoretical (Charpinet *et al.* 1996) and observational (Kilkenny *et al.* 1997; Billères *et al.* 1997) investigations. It consists of hot so-called *horizontal-branch* stars, in the phase of core helium burning, following ignition in a helium flash at the tip of the red-giant branch. Their location at the blue end of the horizontal branch, with effective temperature around 35 000 K, is a result of their having lost most of the original hydrogen envelope. For a recent review, see O’Donoghue *et al.* (1999).

Since their discovery, around 20 members of this group have been detected. The oscillations are excited through the opacity mechanism operating in the opacity bump coming from iron-group elements, likely enhanced by radiatively driven levitation and settling (Charpinet *et al.* 1997). They are characterized by rich spectra of oscillation frequencies, potentially allowing detailed investigations in this late and relatively poorly understood phase of evolution.

Most observations of these stars have been carried out in broad-band photometry. However, recently two groups have succeeded in measuring oscillations in radial velocity. Such

⁶Also known as *EC 14026 stars*, after the first member of the class to be discovered.

observations are potentially very important in providing information about the identification (*i.e.*, the degree and possibly azimuthal order) of the modes. O’Toole *et al.* (2000) observed the star PG 1605+072 and found clear evidence of oscillations in three modes (or groups of modes) in the Balmer lines of hydrogen. The frequencies agreed with those obtained through photometry, with substantially higher frequency resolution, from a multi-site campaign by Kilkenny *et al.* (1999). Interestingly, O’Toole *et al.* found that for a given mode the radial-velocity amplitudes decreased with increasing order in the Balmer series (*i.e.*, decreasing wavelength). This presumably reflects aspects, so far not understood, of the behaviour of the oscillations in the stellar atmosphere. Jeffery & Pollacco (2000) observed the stars KPD 2109+4401 and PB 8783; in the latter case, five or six modes were identified, again agreeing in frequency with modes observed in photometry; the photometric observations show strong evidence for rotational splitting of most of these modes, indicating that they are nonradial. Further spectroscopic observations, with longer time basis, are required to resolve the modes and obtain more precise information about the amplitude and phase relations, for use in the mode identification. Additional information can also be expected from other properties of the spectral lines; an important example is observation of oscillations in equivalent widths.

The rich spectra of oscillation frequencies potentially strongly constrain the properties of the stars, provided the observed frequencies can be identified with modes of stellar models. Even without further observational information about the degrees of the modes, this may be possible through fits of the frequencies to those of models of varying parameters. A very interesting example was provided by the analysis by Brassard *et al.* (2001) of observations of PG 0014+067. Identification of the modes led to stringent constraints on the parameters of the star, including the mass M_{env} of the outer hydrogen-rich layer, which was determined as $\log M_{\text{env}}/M = -4.31 \pm 0.22$. Also, the surface gravity was obtained with a precision of around 2 per cent. Interestingly, the remaining residuals between the observed and fitted frequencies were substantially larger than the observational errors, indicating errors in the model calculations; one might hope that further analysis of these residuals may indicate how the models should be improved, beyond the assumptions of the original calculation.

2.4.4 Pulsating white dwarfs

The first observations of oscillations in white dwarfs were made in 1970 – 1975 (McGraw & Robinson 1976). The initial results were obtained for so-called DA white dwarfs, characterized by the presence of hydrogen in their spectra, with effective temperatures around 10 000 K. Since then, additional groups of pulsating white dwarfs have been detected, each characterized by a fairly sharply defined instability region. These regions are indicated schematically in the HR diagram in Figure 2.17; they include planetary-nebula nuclei variables (‘PNNV’) which are in a stage of rapid evolution.

The typical periods of pulsating white dwarfs are in the range 3 – 10 mins. This is far longer than the dynamical timescales t_{dyn} for these stars [*cf.* equation (1.1)] which are of the order of seconds. In fact, the observed modes are identified with the so-called g modes, *i.e.*, standing gravity waves. As discussed in Chapter 5, such modes may have arbitrarily long periods. As for the δ Scuti stars, it is characteristic that not all the possible modes in a given frequency range are observed; the mode selection is apparently related to the possibility of trapping of modes in regions of chemical inhomogeneity, although the precise mechanism is so far not understood.

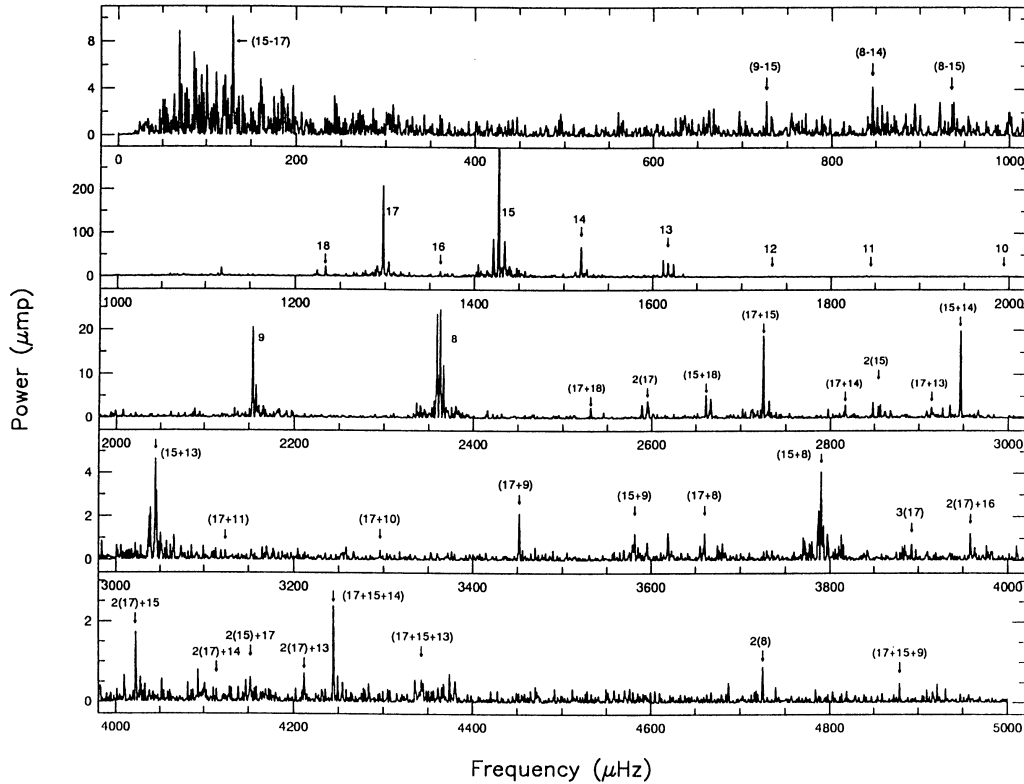


Figure 2.24: Power spectrum of the DB variable GD358, obtained with the Whole Earth Telescope. Numbers with arrows represent multiplet identifications. As discussed in Section 2.2.5, nonlinear effects give rise to linear combinations of the basic frequencies (see also Appendix C, Problem 1.4); these are indicated in the figure as, *e.g.*, ‘(15+18)’ or ‘2(17)’. (From Winget *et al.* 1994.)

The oscillations have been observed photometrically. As in other cases the complications associated with gaps in the data from a single site have led to collaborative efforts to obtain continuous data through the combined efforts of several observatories. This has been organized in the very ambitious Whole Earth Telescope (WET) project, where more than ten observatories have been involved in campaigns to observe a single star over 1 – 2 weeks (for overviews, see Winget 1993; Kawaler 1995). This has led to some of the the most detailed pulsation spectra for stars other than the Sun. As an example, Figure 2.24 shows the spectrum obtained for a DB variable.

The analysis of the observed frequencies is providing a great deal of information about the white dwarfs, such as accurate determination of white-dwarf masses and rotation rates (*e.g.* Bradley & Winget 1994). Metcalfe, Winget & Charbonneau (2001) made a detailed analysis of the frequencies of GD358, resulting amongst other parameters in a determination of the mass fraction of oxygen in the core of the white dwarf; they noted that, when combined with evolution models of the preceding phases of evolution, this constrains the

rate of alpha-particle capture in carbon twelve. Perhaps the most interesting result is the measurement of period changes in white dwarfs, caused by the evolution of the stars along the white-dwarf cooling sequence (*e.g.* Winget *et al.* 1985; Kepler *et al.* 1991). In early stages of the evolution towards the white-dwarf phase the cooling is dominated by neutrino emission from the core of the stars; thus the observations promises to yield information about physical processes involving electrons and neutrinos which cannot be studied experimentally (*e.g.* O'Brien *et al.* 1998; Costa, Kepler & Winget 1999; O'Brien & Kawaler 2000). Measurements of period changes of cooler white dwarfs, in particular the DA variables, may provide a test of the crystallization of matter in the stellar interiors and yield constraints on the overall cooling timescale of white dwarfs (*e.g.* Winget *et al.* 1997). This is crucial for estimates of the age of the Galaxy from the observed distribution in luminosity of white dwarfs (*e.g.* Wood 1992).

